Experimental Investigation and Velocity Statistics in a Taylor-Couette Facility

Student:
Reza Amini Raoofpour
1129491

Supervisor:
Univ.Prof. Dipl.Ing. Dr.Ing. Alfredo Soldati

Co-Supervisors:
Univ.Ass. Marco De Paoli MSc PhD
Projektass. Mobin Alipour MSc

A thesis presented for the Master's degree of
Mechanical Engineering

E322 Institute of Fluid Mechanics and Heat Transfer
Technical University of Vienna
Vienna
12.Jun.2019

Abstract

The flow between two rotating and concentric cylinders is defined as Taylor-Couette Flow. This configuration has been widely studied theoretically, numerically and experimentally because of its relative simplicity and for the implications it can bear in geophysical and industrial applications. In this work, we developed numerical tools to analyse the experimental data obtained via laser doppler anemometry technique.

We performed experiments at low Reynolds number and investigated the regime transition. We analyzed the data in terms of both mean and time dependent quantities and we characterise the transition. In particular, we characterise the time-dependent flow by means of Fourier analysis. Data are processed with the codes developed in this work, which allowed an accurate comparison of the results obtained in correspondence of different Reynolds and Taylor numbers, i.e. different velocities.

Data are processed with in house codes, which allowed an accurate comparison of the results obtained in correspondence of different Reynolds numbers, i.e. different velocities.

Finally, we provide indications for future investigations with the aim of extending the regimes currently observed.

Acknowledgements

I would first like to thank my supervisor Prof. Alfredo Soldati and co-supervisor Dr. Marco De Paoli and Mr. Mobin Alipour of the Institute of Fluid Mechanics and Heat Transfer at the Technical University of Vienna, who helped me academically and gave me the opportunity to work with them. They have invested an incredible amount of time in my work. They was always very friendly and nice to me and i am so grateful to all their effort.

I would like also to thank Univ.Prof. Dipl.-Phys. Dr.rer.nat. Hendrik Christoph Kuhlmann for supporting me throughout the process, and Mr. Haotian Wu Msc, who helped me, whenever i ran into a trouble or had a question about my research.

Finally, I must express my very profound gratitude to my parents and to my lovely wife for providing me with unfailing support and continuous encouragement throughout my years of study and through the process of researching. This accomplishment would not have been possible without them. Thank you all.

Contents

List of Figures

List of Tables

1. Introduction

In nature, a large number of different physical systems can be found, which have transitions far away from the thermal equilibrium, in which their macroscopic behavior in space and time changes dramatically. In general, the structures occurring here, and especially the equations representing them, are extremely complex in such non-equilibrium systems, so that the description of the spatiotemporal structure transitions is qualitatively and quantitatively very difficult. Various models and concepts of nonlinear dynamics should serve to better understand the basic principles of the formation of such structures and patterns. Just as important as crucial is the review of these concepts on the basis of 'simple' experimentally accessible systems. Such a hydrodynamic model system also represents the Taylor Couette system, which is very well suited to study various structure-building phenomena and self-organization processes, as it has a very wide range of different states. Thus, depending on individual system parameters, e.g. boundary conditions or Velocity, it can be found in a wide variety of structures, ranging from laminar flows to spatiotemporal periodic states, to turbulent and chaotic forms.

A major advantage of the Taylor-Couette system as a model system is that the equations necessary for the description, the Navier-Stokes equations (NSE), are well known and perfectly adequate for the qualitative as well as quantitative analysis of the flow fields. This requirement is not necessarily given in most other physical systems. But even here the partial differential equations can only be solved analytically in individual special cases, so that one generally depends on numerical solution methods. A comparison of numerical data with experimental data leads to a further understanding of general structure-forming phenomena. Again, this is an essential point that speaks for the Taylor-Couette system as a model system, since the experimental set-up is relatively easy to implement and there are already many works, both in experiment and in numerics.

The first investigations in the Taylor-Couette system were made more than a hundred years ago, so inevitably the question arises why there is still interest in the investigation of this 'old' system today. The original idea of the system described by G. I. Taylor (Taylor (1923)) at the end of the 19th century was the experimental determination of the viscosity of a fluid as well as the confirmation of the basic hydrodynamic equations. Since then many investigations have been carried out experimentally and numerically, according to this matter that, the rotating turbulent flows are very common and ubiquitous in science and engineering. As example can be mentioned to the flows in propellers ship, jet engines and wind turbines.

Taylor initially found a purely azimuthal flow at low rotational frequencies, the so-called Couette flow, or Circular Couette Flow (CCF), and later at higher rotational frequencies, Taylor vortex, or the Taylor Vortex Flow (TVF). Crucial here was that he could already theoretically predict their existence in the case of periodic boundary conditions. Thus, the initial interest soon changed to an investigation of the different structures occurring in the system and in particular their bifurcation behavior. Today, a large number of different structures are known, such as Spiral Vortex Flow (SPF), wavy vortexes and chaotic Structures. The richness of these diverse flow patterns is illustrated in the experimental work by Andereck et al. (1986), in which a wide variety of different states have been characterized and classified.

A first study on the transition from CCF to wandering waves in the Taylor-Couette finite counter-rotating cylinder system was made by Edwards (1990) and later Edwards (1991) for periodic, nonlinear spirals without periodic pressure and after these experiments the previous calculations always have been used for axially periodic boundary conditions and thus to show a pure axial flow.

1.1 Flow Configuration

Taylor-Couette (TC) cell consists of two Cylinders with same height, but with two different radii and a fluid, which flows in a gap between two cylinders. Each cylinder can rotate independently with a different angular velocity. The geometrical parameters describing the TC cell are inner radius r_0, outer radius r_1, height of cylinder H, radial difference or the gap between cylinders $d = r_1 - r_0$, as reported in (figure 1.1.1).

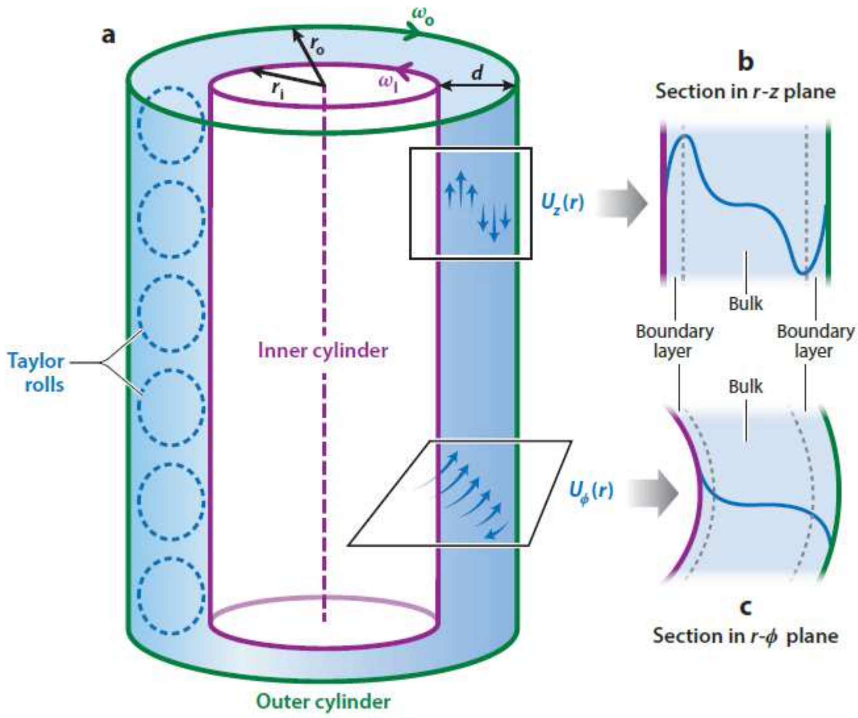

Figure 1.1.1: Sketch of Taylor-Couette flow. The inner and outer cylinder radii are r_0 and r_1, and angular velocities are ω_0 and ω_1,respectively as indicated. Radial difference is $d = r_0 - r_1$, and radial distances from the origin is called r. The mean azimuthal velocity field is $U_\phi(r) = r\Omega(r)$, where $\Omega(r)$ is the angular velocity. The mean axial velocity field is $U_z(r)$, which, besides depending on r, will also depend on the axial position z. The dashed rolls indicate the Taylor roll remnants with axial and radial velocity components, which are considered to be the largest eddies of the turbulent Taylor-Couette flow. (b) The axial velocity and (c) the azimuthal velocity profiles in the boundary layers and the bulk. Courtesy of Grossmann and Lohse (2000).

On the inside and outside of walls in Taylor-Couette cylinder we assume that, we have no-slip boundary conditions. It means that the fluid on the cylinder edge has same velocity of cylinder. The velocity fields are rewritten in cylindrical coordinates:

$$U(r) = U_r e_r + U_\phi e_\phi + U_z e_z \tag{1.1.1}$$

In this case U_r is radial component, U_ϕ azimuthal is tangential component and U_z axial component of velocity field.

In addition to geometric parameters there are also some crucial parameters in dimensionless form. Radius ratio $\eta = r_0/r_1$ and Aspect ratio $\Gamma = H/d$ are two dimensionless parameters related to radii and height of cylinder. Rotation difference of inner and outer cylinder are described by dimensionless parameter Reynolds number. It's for inner cylinder $Re_i = r_i\omega_i d/\nu$ and for outer cylinder $Re_o = r_o\omega_o d/\nu$, where ω_i and ω_o are inner and outer angular velocity of cylinders, respectively, and ν is the kinematic viscosity of flow between two cylinders. It should be also mentioned that Re_0 is always positive for co-rotating outer cylinder and it's negative for counter rotating outer cylinder.

Instead of Re_i and Re_o, Taylor Number Ta is another dimensionless character, which can be also used alternatively for TC flow. In fluid dynamics, the Taylor number Ta is a dimensionless quantity that characterizes the importance of centrifugal "forces" or so-called inertial forces due to rotation of a fluid about an axis, relative to viscous forces, but also in the case of inertial instability such as Taylor–Couette flow, the Taylor number is mathematically analogous to the Grashof number which characterizes the strength of buoyant forces relative to viscous forces in convection. Likewise, in various systems and geometries, when the Taylor number exceeds a critical value, inertial instabilities set in, sometimes known as Taylor instabilities, which may lead to Taylor vortices or cells. The advantage of using the Taylor number rather than the Reynolds number is that the analogy between TC flow and Rayleigh-Bérnard (RB) flow (which will be mentioned in following). Ta is defined in Eq. (1.1.2), according to Grossmann et al. (2016)

$$Ta = \frac{(1+\nu)^4}{64\nu^2} \frac{(r_o - r_i)^2 (r_i + r_o)^2 (\omega_i - \omega o)^2}{\nu^2} \tag{1.1.2}$$

Another alternative dimensionless number is Rossby number Ro. The Rossby number is used in describing fluid flow. The Rossby number is the ratio of inertial force to Coriolis force and the advantage of this representation is that in the coordinate system corotating with the outer cylinder, Ro^{-1} directly characterizes the strength of the driving Coriolis force, as can be seen from the underlying Navire-Stokes equation formulated in that coordinate system. It's defined in Eq (1.1.3) by Grossmann et al. (2016):

$$Ro^{-1} = \frac{2\omega_o d}{|\omega_i - \omega_o| r_i} = -2\frac{1-\eta}{\eta}\frac{a}{|1+a|} \tag{1.1.3}$$

where rotation ratio is $a = -\omega_o/\omega_i$ with $a > 0$ for counter rotating and $a < 0$ for co-rotating.

Now and with the knowledge of existing formulas for TC one question could be arised, which is about the flow features with increasing driving strength. As it shown in figure 1.1.2 it can be obtained, when Taylor numbers are still low ($Ta \approx 10^6$; see figure 1.1.2a), coherent structures are present in the gap between cylinders. These structures make up Taylor rolls, also called Taylor vortices, shown in figure 1.1.1, and as long as Ta increases, those structures length scale decreases. Around $Ta \approx 10^6$ the coherence length of these structures start to become smaller than the gap between cylinders (the gap width d), and exactly at this point turbulence starts to develop in the bulk between the inner and outer cylinders. At the same time the boundary layers are starting to develop with the properties, with different form from the bulk flow. The boundary layers have still properties of laminar type, which can be described by the Prandtl-Blasius theory. This regime calls the classical regime of TC turbulence, that in figure 1.1.2b a snapshot of the azimuthal velocity profile in this regime has been presented.

However, around $Ta \approx 3 * 10^8$ (for $\eta = 0.71$), the situation changes drastically, as then the boundary layers are sheared strongly enough to undergo a shear instability and become turbulent (i.e., of the Prandtl–von Kármán type). This regime, shown in Figure 1.1.2c, is called the ultimate regime of TC turbulence. Note that at this transition, the bulk flow does not change much: Depending on Ro^{-1}, it either is still featureless (for positive Ro^{-1}, meaning corotation) or features Taylor rolls—either over the full bulk area (the gap width minus the boundary layers) or, because of the stabilization by strong counter-rotation of the outer cylinder, only close to the inner cylinder. In addition, the statistics of the turbulent fluctuations in the bulk change only quantitatively beyond the transition toward the ultimate regime, with the inertial regime increasing in size Grossmann et al. (2016).

As shown in figure 1.1.1 TC cell is a closed symmetric system with a simple geometry, and these features make flow in TC very similar to the flow in Rayleigh-Bérnard (RB), which consists flow in a box, that heated from bottom, and cooled from above. Both these paradigmatic systems have been investigated numerically and experimentally widely to drive new concepts in world of fluid mechanics, such as: Instabilities Chandrasekhar (1981) Pfister and Mullin (1988), pattern formation Andereck et al. (1986) Pfister and Mullin (1988), turbulence Grossmann and Lohse (2000) Lohse and Xia (2010). In TC and RB there is a complete-defined relationship between input energy and energy dissipation rate. The amount of power entered into the flow is directly connected to the global fluxes, and for TC this input power is angular velocity transport from inner cylinder to outer cylinder, and for RB is the heat transport from bottom side to the above side. So we just have to measure only one global quantity, which is the required torque for rotating the inner cylinder at constant velocity in TC case, and required heat flux through the

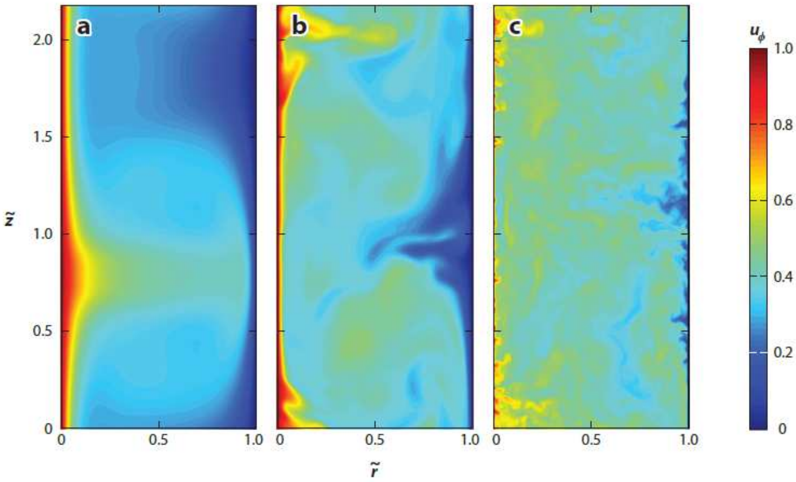

Figure 1.1.2: Snapshots of the azimuthal velocity for pure inner cylinder rotation $Ro^{-1} = 0$ and $\eta = 0.714$. Periodic boundary conditions in the axial direction were used, and $\tilde{r}$ = r/d and $\tilde{z}$ = z/d. (a) $Ta = 7 * 10^5$, (b) $Ta = 5 * 10^7$, and (c) $Ta = 4 * 10^9$. Courtesy of Grossmann et al. (2016)

box for keeping the top and bottom side at constant temperature for RB case. In both cases the total energy dissipation follows from the global energy balance B. Eckhardt and Lohse (2007). Therefore both system can be built in a simple way, but with high precision.

In the 1980s, many investigation have been done on the TC flow, and also on RB flow at the beginning phase of instabilities and beyond of that for small Reynolds number. For small Reynolds number or in other word for a low rotation rate, flow in TC follows rules of circular path in symmetric mode as it has been already expected. This flow is defined as Couette flow. If the rotation rate of inner cylinder exceeds the critical value, then the flow undergoes in an other various transition, which called Taylor vortices, and with further increasing the rotation rate of inner cylinder flow becomes finally turbulent as described in Phase diagram of (Andereck et al., 1986), and you can see it in figure1.1.3. This transition into turbulent is analogue to the transition in RB Chandrasekhar (1981).

In last decades many researches have been done on the flow in RB experimentally and numerically from low Rayleigh number (Ra) to high Rayleigh number Ra=10^{11},[17] Van Gils et al. (2011), which is well beyond onset of turbulence. However, TC flow received less attention, with one exception being the Austin-Maryland experiment by Lathrop and Swinney (1992a) Lathrop and Swinney (1992b) Lewis and Swinney (1999), which explored a pure inner cylinder rotation up to Re=10^6 with outer cylinder at rest, and also Turbulent TC experiments get even more scarce for TC flow with inner and outer cylinders rotating independently. We are only aware of the Wendt experiments in the 1930s, reaching $Re_i \approx\ 10^5$ and $Re_0 \approx \pm 10^5$ and the recent ones by Ravelet et al., reaching $Re_i \approx 5 \times 10^4$ and $Re_o = \pm 2 \times 10^4$.

This situation has been changed in the last decade, and many experiments and researches have been explored on the TC flow. Various Apparatus have been built with independently rotation of inner and outer cylinder in co-rotation or counter rotation direction according to the different Reynolds number. As it shown in tables 1.1, 1.2, 1.3 10 different experiments during the years between 1986 untill 2012 are gathered with details about geometrical parameters,inner and outer angular velocities, inner and outer Reynolds number,Taylor and Rossby numbers and finally shear Reynolds number, which is (Tokgoz et al., 2012)

$$Re_s = \frac{2 \mid \eta Re_o - Re_i \mid}{1+\eta} \tag{1.1.4}$$

Comparing these tables we can figure out, the procedure of increasing shear Reynolds number due to the carried out mentioned experiments over the years.

As mentioned earlier, the Taylor-Couette system has a very large number of different structures. For this reason, only a brief overview of the area of existence, spatiotemporal behavior

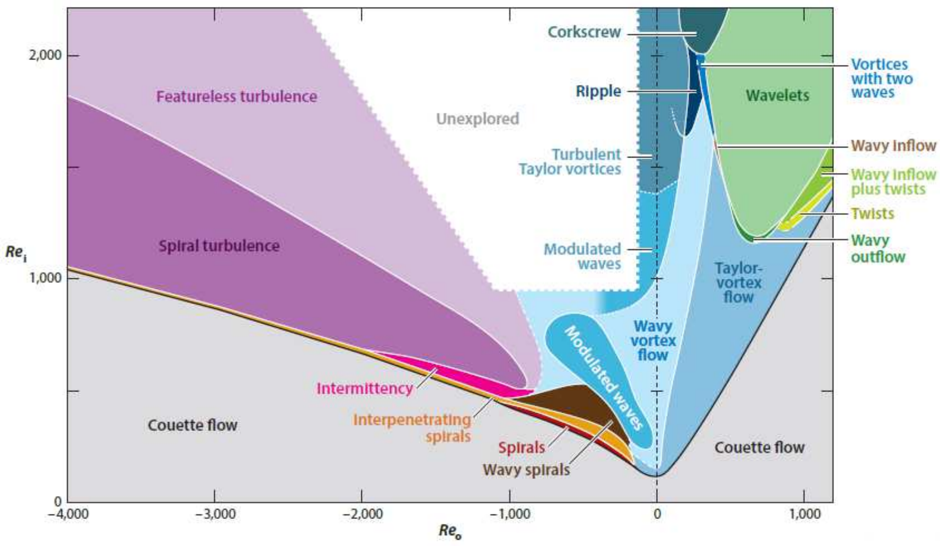

Figure 1.1.3: Flow structures in the (Re_o, Re_i) phase diagram for Taylor-Couette flow at $\nu = 0.833$. Figure taken from Andereck et al. (1986).

and the stability of different solutions can and should be given here. As it has been described in chapter 2 we did some investigations on a Taylor-Couette cylinder over some of these areas, and then we have studied the structure of flow in these areas in qualitative and also quantitative way. The quantitative measurement are carried out with Laser-Doppler Anemometer (LDA) as it reported in subsection 2.2.1. In the next sections of this chapter we describe, how the captured data from experiment could be examined, prepared and import to the program MATLAB for further steps.

The structures of interest for this work are described more in detail in Chapter 3. All the results have been categorized and classified as qualitative and quantitative results.

#	r_i $[m]$	r_o $[m]$	H $[m]$	d $[m]$	Γ	η	References
1	0.2	0.2794	0.927	0.0794	11.675	0.716	Van Gils et al. (2011)
2	0.035	0.07	0.7	0.035	20	0.5	Merbold et al. (2013)
3	0.16	0.22085	0.695	0.06085	11.42	0.724	Paoletti and Lathrop (2011)
4	0.0525	0.05946	0.33408	0.00696	48	0.883	Andereck et al. (1986)
5	0.0525	0.05946	0.2088	0.00696	30	0.883	Andereck et al. (1986)
6	0.04	0.08	0.41	0.04	10.250	0.5	Stefani et al. (2006)
7	0.11	0.12	0.22	0.01	22	0.917	Tokgoz et al. (2012)
8	0.11	0.12	0.22	0.01	22	0.917	Tokgoz et al. (2012)
9	0.2	0.2794	0.927	0.0794	11.675	0.716	Van Gils et al. (2012)
10	0.2	0.2794	0.927	0.0794	11.675	0.716	Van Gils et al. (2012)
11	0.053	0.06	0.18	0.007	25.714	0.8833	Present Study

Table 1.1: Geometrical parameters. Table of 10 difference experiments of TC. r_i is inner radius. r_o is outer radius. H is height of cylinder. d radial difference. Γ is aspect ratio. η is radius ratio.

#	ω_i $[s^-1]$	ω_o $[s^-1]$	ν $[m^2/s]$	Fluid Type	References
1	125.6	62.8	1×10^{-6}	Water	Van Gils et al. (2011)
2	530.66	76.616	6.80×10^{-7}	Silicone Oils	Merbold et al. (2013)
3	125.6	62.8	5.50×10^{-7}	Water	Paoletti and Lathrop (2011)
4	5.4735	9.6655	1×10^{-6}	Water	Andereck et al. (1986)
5	2.8462	1.7398	1×10^{-6}	Water	Andereck et al. (1986)
6	0.3768	0.1017	3.4×10^{-7}	$Ga^{67}In^{20.5}Sn^{12.5}$	Stefani et al. (2006)
7	20.42	-18.72	9.6×10^{-7}	Water	Tokgoz et al. (2012)
8	4.78	-4.39	9.6×10^{-7}	Water	Tokgoz et al. (2012)
9	16.3	-32.6	1×10^{-6}	Water	Van Gils et al. (2012)
10	85.7	17.1	1×10^{-6}	Water	Van Gils et al. (2012)
11	26.954	0	2×10^{-5}	Baysilone $M20$	Present Study

Table 1.2: Kinematic and fluid parameters. Table of 10 difference experiments of TC. ω_i is angular velocity of inner cylinder. ω_o is angular velocity of outer cylinder. ν is kinematic viscosity.

#	Re_i	Re_o	Ta	Ro^-1	Re_s	References
1	1.99×10^6	1.39×10^6	1.51×10^{12}	0.794	1.16×10^6	Van Gils et al. (2011)
2	9.56×10^5	2.76×10^5	1.91×10^{12}	0.337	1.09×10^6	Merbold et al. (2013)
3	2.22×10^6	1.53×10^6	1.84×10^{12}	0.761	1.29×10^6	Paoletti and Lathrop (2011)
4	2×10^3	4×10^3	2.69×10^6	0.611	1.63×10^3	Andereck et al. (1986)
5	1.04×10^3	7.2×10^2	1.87×10^5	0.417	4.29×10^2	Andereck et al. (1986)
6	1.77×10^3	9.57×10^2	4.77×10^6	0.739	1.72×10^3	Stefani et al. (2006)
7	2.34×10^4	-2.34×10^4	2.21×10^9	-0.087	4.68×10^4	Tokgoz et al. (2012)
8	5.48×10^3	-5.49×10^3	1.21×10^8	-0.087	1.10×10^4	Tokgoz et al. (2012)
9	2.59×10^5	7.23×10^5	9.16×10^{11}	-0.529	9.05×10^5	Van Gils et al. (2012)
10	1.36×10^6	3.79×10^5	1.80×10^{12}	0.198	1.27×10^6	Van Gils et al. (2012)
11	500	0	3.3×10^4	0	1.13×10^3	Present Study

Table 1.3: Dimensionless parameters. Table of 10 difference experiments of TC. Re_i is inner Reynolds number. Re_o is outer Reynolds number. Ta is Taylor number. Ro^-1 is Rossby number. Re_s is shear Reynolds number.

2. Methodology

The main aim of experiment is, at the first step, to investigate the rotating flow by mean of disposed particles. The interplay between flow and particles are complicated and they count on diverse parameters, as the rate of diameter of particle to a typical length scale of the flow and the concentration of particles.

First important and basic investigation regarding to interaction between particles and rotating flow or in other word stability of a liquid between two rotating cylinders, which is exactly corresponding to our investigation, was published by Taylor (1923) and as it mentioned in last chapter, when the Taylor number is increased beyond a critical value the basic flow changes to a system of regular vortices. If the Taylor number is further increased, other stable flow structures arise, up to the transition to turbulence.

In the following subsections first the procedure of our investigation by Taylor-Couette cylinder will be explained, then captured data methodology by the laser (Laser Doppler Anemometry) will be shown and discussed, and finally data analysis process by the program MATLAB in details will be reported.

2.1 Experimental Setup

Taylor examined flows in the concentric gap between two, because it's much more easier to design a apparatus and study the flow of fluid under pressure through a tube or a flow in the concentric gap between two cylinders. In our experiment, as it illustrated in figure 2.1.1, we used a Taylor-Coutte Cylinder with inner radius $r_i = 53mm$, outer radius $r_o = 60mm$ and height of cylinder $H = 180mm$ as geometrical parameter and in the gap between two cylinders we used Baysilone Fluids M20 [see appendix] with kinematic viscosity $\nu = 20mm^2.s^{-1}$, density $\rho = 0.95g.cm^{-3}$ at temperature 25°C and Aluminum flakes particles [See appendix].

With knowing this information about geometrical parameters and also kinematic viscosity ν we define Taylor number Ta and Reynolds number Re for our Taylor cylinder, respectively.

$$Ta = \frac{\Omega_i^2 r_i (r_o - r_i)^3}{\nu^2}\,, \tag{2.1.1}$$

$$Re = \frac{\Omega_i r_i (r_o - ri)}{\nu}. \tag{2.1.2}$$

Also another defined dimensionless number by Taylor (1923), which is related to our case, is critical Taylor number as you can see bellow:

$$T_c \approx 1708 \left[1 + 0.652 \left(1 - \frac{r_i}{r_o} \right) \right]. \tag{2.1.3}$$

When the Taylor number is increased beyond a critical value the basic flow changes to a system of regular vortices. If the Taylor number is further increased, other stable flow structures arise, up to the transition to turbulence.

After getting used with the apparatus, and attention to all instruction we began to work with, and we did set the Taylor Cylinder to run for 16 different times, every time for a different Reynolds number. Also we observed that the temperature in all steps should be kept at 25°. The system data are illustrated in table 2.1. But it should be said, that all the illustrated data, and what has been mentioned about increasing the Ta did correspond completely with the equation 2.1.3. Because in our case the T_c is equal to 1837.925, and with increasing the Taylor number

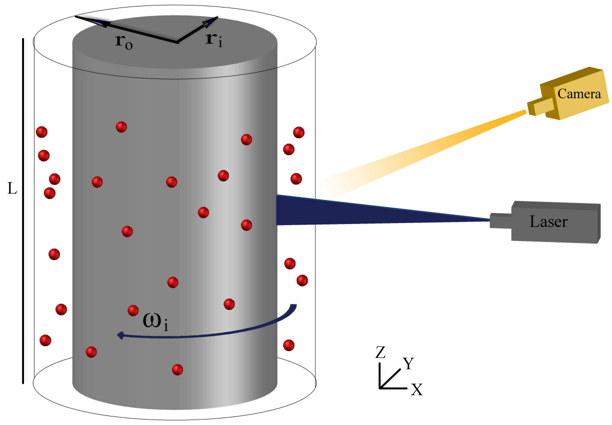

Figure 2.0.1: Schematic of the Taylor-Couette setup. Two concentric cylinders of radii r_i and r_o with a working fluid in between. The inner cylinder rotates with angular velocity ω_i, while the outer cylinder is kept at rest. The coordinate system is given by X for radial, Y for azimuthal and Z for axial direction. The laser Doppler anemometry (LDA) probe is positioned at mid height to measure the velocity at mid gap.

exactly in the next step of our experiment at $Ta = 1862.470$ ($Re = 118.75$) we have observed, that flow changed to a system of regular vortices, and with more increasing the Taylor number other stable flow structures have been arises, as it mentioned before. However, we will discuss about this with details in next chapter.

2.2 Quantitative measurements

The flow structures are examined qualitatively as well as quantitatively. Qualitative investigations are conducted by visualization techniques. Suitable particles are added to the oil, which is used as experimental fluid. The movement of the particles can be observed with the help of a thin halogen light sheet. Quantitative measurements we carried out with Laser-Doppler-Anemometer (LDA), and in following quantitative measurement with LDA will be described.

2.2.1 Laser Doppler Anemometry (LDA)

Laser LDA, which is also known as Laser Doppler Velocimetry (LDV) is an optical method used to measure the velocity field for non-intrusive 1D, 2D and 3D point in free flows and internal flows. LDA System has been used widely for industrial and scientific purposes for gaining a better and clearer understanding of fluid mechanics. Also in product design and to modify aerodynamic efficiency, quality and safety the measurement results have very important role.

The Laser Doppler Anemometer, or LDA, is a widely accepted tool for fluid dynamic investigations in gases and liquids and has been used as such for more than three decades. It is a well-established technique that gives information about flow velocity. It's non-intrusive principle and directional sensitivity make it suitable for applications with reversing flow, chemically reacting or high-temperature media and rotating machinery, where physical sensors are difficult or impossible to use. It requires tracer particles in the flow. The method's particular advantages are: non-intrusive measurement, high spatial and temporal resolution, no need for calibration and the ability to measure in reversing flows (Dantec-Dynamics, 2000).

As you can see in figure 2.2.2 an LDA system consists at first a resonator, that radiats a wave laser, then the continuous wave will be split by beam splitter and with help of focusing lens waves transmitted to the flow, which is seeded with particles. As beam splitter, in most of times a Bragg cell is used. Bragg cell is glass crystal with a attached vibrating piezo crystal. The vibration generates acoustical waves acting like an optical grid. The output of the Bragg cell is two beams of equal intensity proportional to the angle between two beams in probe volume,

Figure 2.1.1: Taylor Cylinder cell used for the present investigation.

wavelength and moving direction of particle in flow as you can see in equation 2.2.1:

$$I \propto 1 + \cos\left[2\pi \frac{2\sin\theta/2}{\lambda} x\right]. \tag{2.2.1}$$

These outputs from Brag cell are focused into optical fibres bringing them to a probe. In the probe, the parallel exit beams from the fibres are focused by a lens to intersect in the probe volume. Then this transmission will be received by focusing lens and after passing from an interference filter will be leaded to photodetector and then to the signal conditioner and signal processor for further analyzing and processing.

About the operation of LDA on the probe volume as shown in figure 2.2.3 two laser beams cross at a small angle. A laser is coherent, which means that the light is all in phase, i.e. the peaks and troughs of the waves are aligned, and the peaks of the wavefronts are shown as the thin lines in each beam. When the two beams cross in the geometry shown we see that there

(a) Picture from LDA Laser.

(b) Picture from Laser beam while focusing on the Cylinder.

Figure 2.2.1: Captured Pictures during the Experiment.

Number	ω_i $[rad/s]$	Re	Ta	Speed of Rotation $[rpm]$	Regime
1	2.695	50	330	26.49	CCF
2	4.043	75	743	40.14	CCF
3	5.390	100	1320	52.95	CCF
4	6.064	112.5	1671	60.13	CCF
5	6.401	118.75	1862	63.45	TVF
6	6.738	125	2064	66.80	TVF
7	7.412	137.5	2497	73.42	TVF
8	8.086	150	2971	79.20	TVF
9	9.433	175	4045	93.35	WVF
10	10.781	200	5282	105.90	WVF
11	13.477	250	8254	131	WVF
12	16.172	300	11886	157	WVF
13	18.867	350	16177	184	WVF
14	21.563	400	21144	209	WVF
15	24.258	450	26743	238	WVF
16	26.954	500	33018	260	WVF

Table 2.1: Table of 16 difference experiments on the TC and the obtained Results. ω_i is angular velocity of inner radius. Re is Reynolds number. Ta is Taylor number. Speed of rotation [rpm]= $(\omega_i * 60)/2\pi$. CCF is Circular couette Flow, TVF is Taylor vortex flow, and WVF is Wavy vortex flow.

is an interference pattern that exists with the wavefront peaks and troughs of the two beams aligning in the horizontal direction (the peaks are shown by the bold green lines). This pattern is stable in space even though both waves are propagating. This produces parallel planes of high light intensity, so called fringes and the spacing of the fringes is given by d_{fringe}, and it's equal to (Engine-Research-Center (2015)):

$$d_{\text{fringe}} = \frac{\lambda}{2 * \sin\theta/2}. \tag{2.2.2}$$

Consider now a particle so small that its inertia is negligible and it travels with the same velocity as the fluid, V. When the particle traverses the intersection region of the two beams which called already the probe volume it scatters light from the stationary fringes. The y-component of velocity causes the particle to cross the fringes giving rise to an oscillating signal in time. The time between peaks in the scattered light T_D corresponds to the time that it takes a particle to travel dfringe. Very simply then, the velocity is dfringe divide by the period of the scattered light oscillation as you can see below [Engine-Research-Center (2015)]:

$$V_{P_\perp} = \frac{d_{\text{fringe}}}{T_D}. \tag{2.2.3}$$

2.3 Experiment Setup and Calibration

In the last section we have discussed about main components of Taylor-Couette Cell and LDA system, how to measure the velocity field by Laser beams and Camera, and capturing the results by system. In next section we will discuss about the captured results by system and describing about importing the data into MATLAB program, analyzing them, and finally about the output, that we get.

2.3.1 Data Acquisition

During experiments and after dealing with LDA system we could get the results in two different forms but in the same text format as you can see following in figure 2.3.1.

As it shown in figure 2.3.1(a) we have data related to the Re=175. In this step first we have focused by laser beam on the middle of cylinder, as it mentioned in last section, and we have

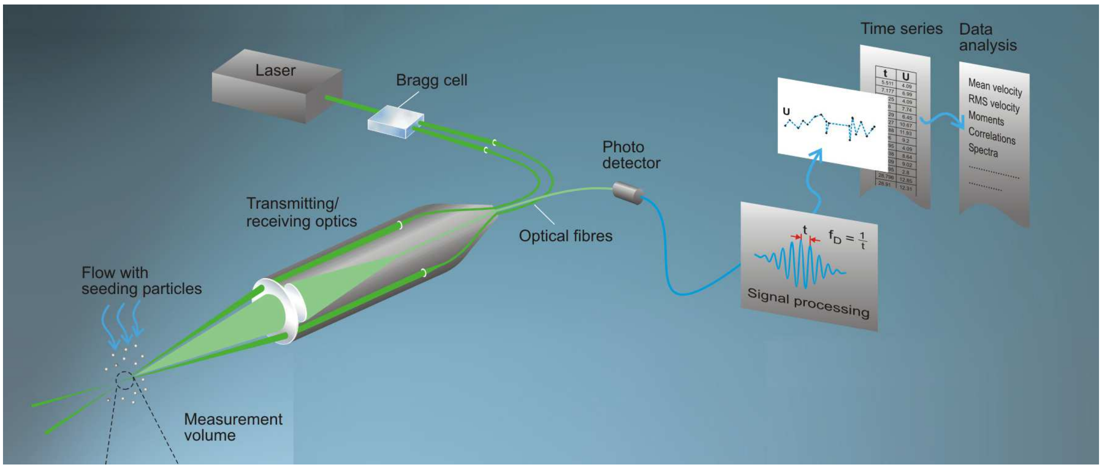

Figure 2.2.2: LDA Principle. Here we show wave laser: after exit from Resonator and passing from BraggCell will be splitted, then outputs should have been focused by the lens in the transmitting on the probe volume, and at the end this transmission will be received and leaded to the Photo detector for further processes.Courtesy of [Dantec-Dynamics (2000)]

calibrated the cell in X direction from 0 to 10, in Z direction from -60 to 60. Then we moved the beam in X direction at three points 2, 4 and 6 from -60 till 60 in Z direction, without any move in Y direction. But we did set the laser beam to move and capture the data on the Z direction just at the paired points (-60:2:60). It means in every Reynolds Number we have Matrix with 183 rows and 15 columns. In part (b) we just considered the coordination X = 4, Y = 0, and Z from 30 till -30 (30:-2:-30). But in this case we just measuring the instantaneously velocity on every single point instead of measuring the mean velocity in all of points, and it gives us one matrix with more than 8550 rows and 6 columns.

To import the data in MATLAB we had to write a command, that first turn all ',' to the '.' then turn all ';' to space and finally removing the first five sentences, because these are not related to our work, and the remaining result would be saved as Matrix in MATLAB as it shown below:

```
lsor_result = zeros(31, 1501);          % defining a zero Matrix with 31 rows & 1501 columns
psor_result = zeros(1501, 31);          % defining a zero Matrix with 1501 rows & 31 columns
s = struct;                             % defining a structure array
counter = 0;                            % defining a counter
for n = -30:2:30                        % definition of input data
    counter = counter +1;
    n_string = num2str(n);
    filename = strcat('x4z',n_string);% concatenating 'x4z' & n_string for defining the filename
    disp(filename)
    Data = fileread(strcat(folder, '\', filename, '.txt')); %reading the file
    Data = strrep(Data, ',', '.');      % changing the ',' to the '.'%
    FID = fopen('A.txt', 'w');          % saving the new file as A.txt
    fwrite(FID, Data, 'char');
    fclose(FID);
    Data = fileread('A.txt');           % reading the new A.txt file
    Data = strrep(Data, ';', ' ');      % changing all ';' to the space
    FID = fopen('B.txt', 'w');          % saving the new file as B.txt
    fwrite(FID, Data, 'char');
    fclose(FID);
    M = dlmread('B.txt',' ',5,0);       % removing 5 first lines from the B.txt
    s(counter).file_name = filename;    % defining file_name as the first field of structure
```

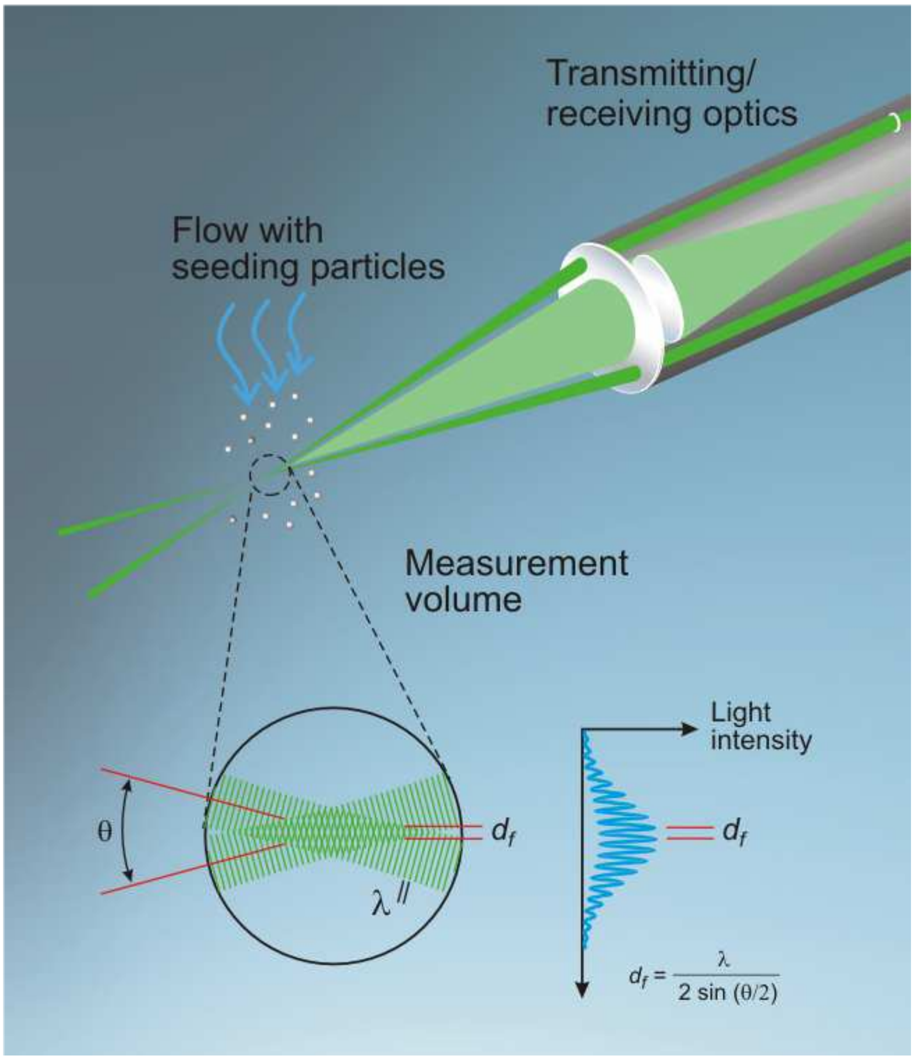

Figure 2.2.3: The Probe Volume is made up of two laser beams crossing each other with angel θ. The probe volume is typically a few millimeters long. The fringe distance d_f is defined by the wavelength of the laser light and the angle between the beams. Courtesy of [Dantec-Dynamics (2000)]

2.3.2 Fast Fourier Transform (FFT)

Object of importing Data in MATLAB has been done and for all of text files we have a related saved Matrix. When we take a over look to the saved Matrix, specially to the Matrix with presenting instantaneously velocity we can figure some graphs out, and all of these graphs show how a signal changes over time or in other words they are defined in the time-domain but for a precise and mathematics discussion we have to convert a time-domain graph to the frequency-domain graph, whereas a frequency-domain graph shows how much of the signal lies within each given frequency band over a range of frequencies.

As you can see in figure 2.3.2 we have a transform from time to frequency and in this transform we defined some variable as:

- Sampling Rate (Fs): Number of data samples acquired per second.
- Frame Size (T): Amount of time data collected to perform a Fourier transform.
- Block Size (N): Total number of data samples acquired during one frame for time domain.

For frequency domain we have also defined variable as Siemens (2019):

- Bandwidth (Fmax): Highest frequency that is captured in the Fourier transform, equal to half the sampling rate.

```
DXEX v1
E:\Documents and Settings\Labor\Desktop\Expeiment at 06.Nov\Reza.lda
No date/time available.
2,00 mm;0,00 mm;60,00 mm
"X [mm]";"Y [mm]";"Z [mm]";"Count{1}";"Count{2}";"Data Rate{1} [#/s]";"Data Rate{2} [#/s]";
"BSA1 Vel-Mean [m/s]";"BSA2 Vel-Mean [m/s]";"BSA1 Vel-RMS [m/s]";"BSA2 Vel-RMS [m/s]";
"BSA1 Vel-MeanConf [m/s]";"BSA2 Vel-MeanConf [m/s]";"BSA1 Vel-RMSConf [m/s]";"BSA2 Vel-RMSConf [m/s]"
2,00;0,00;60,00;1026;44;205,55;8,78;-0,004835;-0,6867;0,02424;0,04707;0,00;0,01;0,00105;0,00995
2,00;0,00;58,00;1002;24;200,31;5,94;-0,004075;-0,7209;0,02245;0,04151;0,00;0,02;0,00098;0,01200
2,00;0,00;56,00;1099;20;220,15;5,47;-0,000426;-0,7196;0,02434;0,03276;0,00;0,01;0,00102;0,01042
2,00;0,00;54,00;1028;48;204,40;10,03;0,000526;-0,7073;0,02302;0,06143;0,00;0,02;0,00100;0,01242
2,00;0,00;52,00;1032;70;205,49;14,40;0,002154;-0,6842;0,02440;0,06227;0,00;0,01;0,00105;0,01039
2,00;0,00;50,00;933;80;186,74;16,31;0,006498;-0,6515;0,02487;0,07163;0,00;0,02;0,00113;0,01117
2,00;0,00;48,00;1193;98;238,30;20,38;0,002358;-0,6411;0,02476;0,07633;0,00;0,02;0,00099;0,01074
2,00;0,00;46,00;893;119;178,69;24,28;0,004768;-0,6248;0,02617;0,07423;0,00;0,01;0,00121;0,00947
2,00;0,00;44,00;855;133;172,67;26,79;0,005581;-0,6006;0,02424;0,07578;0,00;0,01;0,00115;0,00914
2,00;0,00;42,00;1105;146;221,06;29,22;0,002139;-0,5845;0,02457;0,06996;0,00;0,01;0,00102;0,00805
2,00;0,00;40,00;1100;150;222,30;30,02;-0,003077;-0,5918;0,02456;0,08172;0,00;0,01;0,00103;0,00928
```

(a) First Type of text file captured from experiment on Taylor-Couette Cell. Data Rate means Valid signal recorded per second. Vel-Mean means Velocity-Mean. Vel-RMS means Velocity-Root mean square. Vel-MeanConf means Velocity-Mean Confidence interval. Vel-RMSConf means Velocity-Root mean square Confidence interval.

```
DXEX v1
E:\Documents and Settings\Labor\Desktop\Expeiment at 06.Nov\Reza.lda
No date/time available.
4,00 mm;0,00 mm;0,00 mm
"BSA1 Vel [m/s]";"BSA1 TT [us]";"BSA1 AT [ms]";"BSA2 Vel [m/s]";"BSA2 TT [us]";"BSA2 AT [ms]"
0,00;138,7;0,341;-0,04;122,7;1,088
-0,01;128,0;4,437;0,02;13,3;1,621
0,00;128,0;6,997;-0,01;45,3;1,899
0,01;10,7;8,192;-0,03;40,0;3,947
-0,00;64,0;55,552;-0,00;49,3;4,331
0,00;245,3;61,696;-0,00;24,0;5,056
0,00;384,0;66,816;-0,00;6,7;5,184
-0,00;53,3;90,197;-0,03;58,7;5,632
-0,00;202,7;100,352;-0,03;22,7;7,019
0,00;1824,0;166,656;-0,02;40,0;8,256
-0,00;768,0;189,355;0,01;37,3;8,832
0,01;1632,0;190,805;0,02;98,7;10,112
```

(b) Second type of text file captured from experiment on Taylor-Couette Cell. Vel means instantaneous velocity.

Figure 2.3.1: Examples of two different text file obtained from experiment on Taylor-Couette Cylinder.

- Spectral Lines (SL): After Fourier transform the total number of frequency domain samples.
- Frequency Resolution (Δf): Spacing between samples in the frequency domain.

A frequency-domain representation can also include information on the phase shift that must be applied to each sinusoid in order to be able to recombine the frequency components to recover the original time signal. For this matter and converting the time-domain signal into frequency-domain as mentioned we need a transform function which is called Fast Fourier Transform or command FFT in MATLAB.

In MATLAB the function fft, which we can call as Y=fft(X) computes the discrete Fourier transform (DFT) of X using a fast Fourier transform (FFT) algorithm, and this transform is defined as follow:

$$Y(k) = \sum_{j=1}^{n} X(j) W_n^{(j-1)(k-1)}\,, \tag{2.3.1}$$

where $W_n = e^{(-2\pi i)/n}$ is one of the n roots of unity, k = 0,...,N-1, and n is transform length. As you can see in details below and for taking the advantages of defining function fft in MATLAB, we have to define Fs as sampling frequency, and it should be at least twice higher than incoming signal, t as time domain signal, and L as length of signal.Then we continue with writing a program with Computing the two-sided spectrum P2. Then compute the single-sided spectrum P1 based on P2 and the even-valued signal length L.

```

    s(counter).matrix = M;          % defining matrix as the second field of
                                      structure
    y4 = s(counter).matrix(:,4);  % selecting fourth column of saved matrix
    L = numel(y4);                  % defining length of signal equal to number of
                                      elements in y4
```

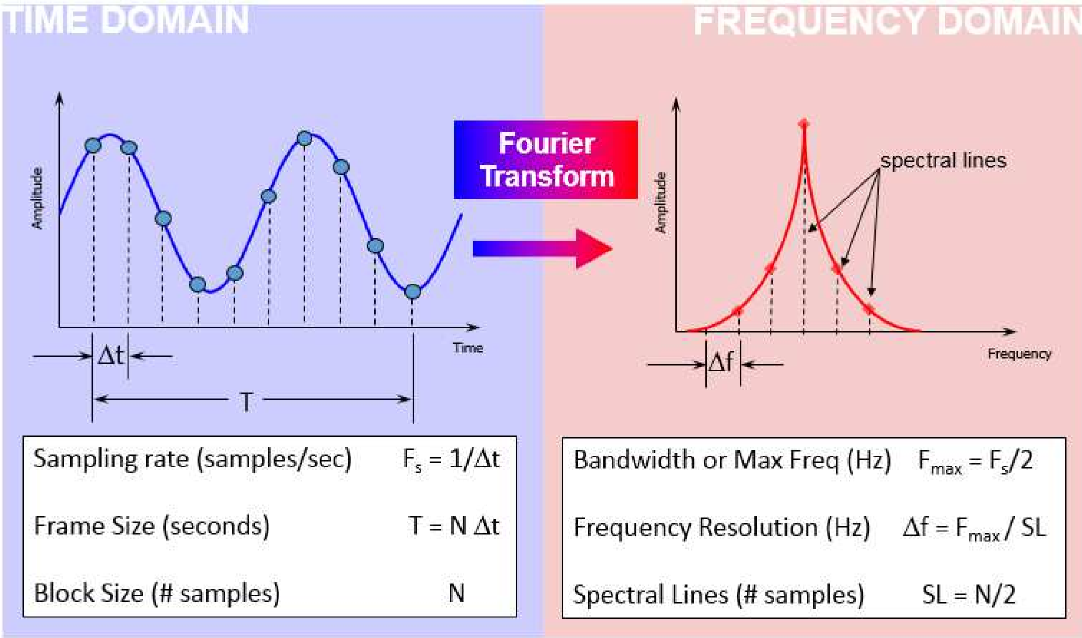

Figure 2.3.2: Time domain and frequency domain terms used in performing a digital fourirer Transform. Courtesy of [Siemens (2019)]

```
t = 1:1:L;                          % time domain signal
Fs = 300;                           % t(2)-t(1)(sampling frequency)
Y = fft(y4);                        % Compute the fast Fourier transform of the signal
f = Fs*(0:(L/2))/L;                 % defining the frequency domain f
P2 = abs(Y/L);                      % Compute the two-sided spectrum P2 Then compute the single-sided spectrum P1 based on P2
P1 = P2(1:L/2+1);                   % compute the single-sided spectrum P1 based on P2 and the even-valued signal length L
P1(2:end-1) = 2*P1(2:end-1);
s(counter).fp = [f ; P1'];          % defining third field of structure as fp with using f & P1
```

Also in figure 2.3.3 and the written command related to the figure 2.3.3 you can observe that in our case, and using the command fft (Fast Fourier Transform) in MATLAB we can create diagram related to the Reynolds Number Re = 300 and detecting the all peak points sorted in descending order, but it should be told that for finding the peak points the command "MinPeakDistance" has been used. It means to improve our estimation of the cycle duration, peaks that are very close to each other have been ignored, and now the acceptable peak-to-peak separations would be restricted to values greater than 0.01.

```
plot(f,P1,'o')                                          % plot a figure according to amplitude & frequency

[psor,lsor] = findpeaks([0; P1],[-0.1 f],'SortStr','descend'); % finding peak points & sorting as descend

findpeaks([0; P1],[-0.1 f],'MinPeakDistance', 0.01) % Improving estimation of the cycle duration by ignoring peaks that are closer than 0.01 to each other

text(lsor -0.1,psor,num2str((1:numel(psor))'))

title('Single-Sided Amplitude Spectrum of S(t)')
xlabel('f (Hz)')
ylabel('|P1(f)|')
```

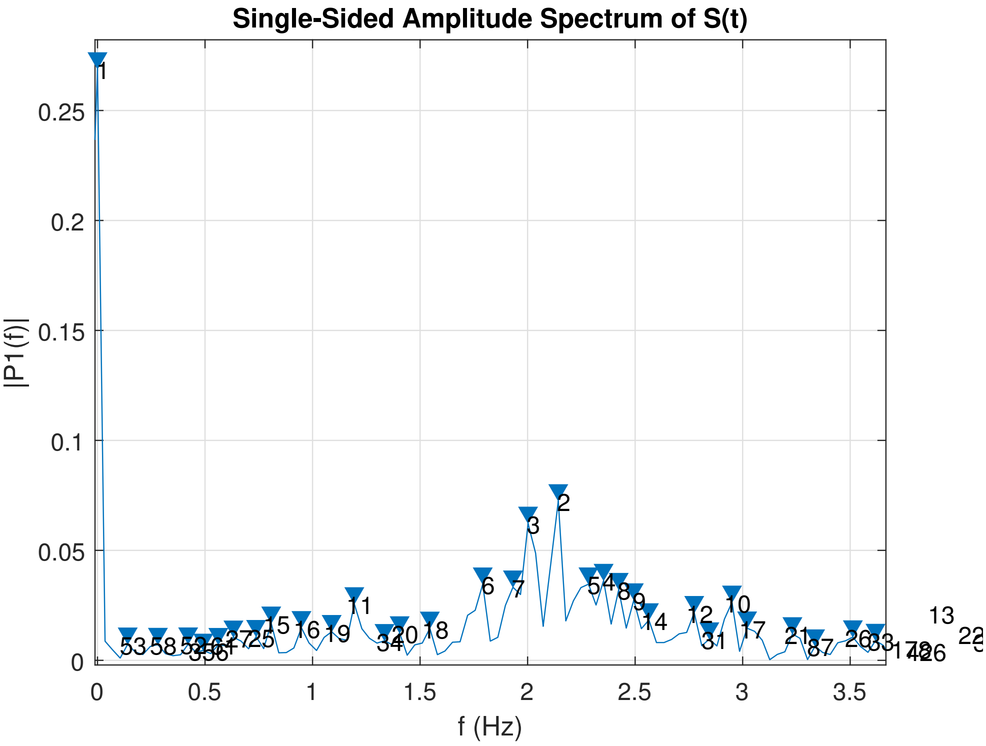

Figure 2.3.3: Captured Diagram with detected Peak Points in assortment Frequency and Amplitude.

3. Results

In this chapter all the results from our experiments will be shown and then described first in a qualitative way and then in a quantitative way. Also all the images from different regimes, which we have been faced with, would be shown. But before this matter first we have to understand all these distinguished regimes according to phase diagram 1.1.3 and velocity fields and other properties in them as well.

3.1 Basic Equation

The starting point for calculating the velocity fields are the equations, that are known as balance equation for mass and momentum. In this case and as you can see in the following we start with writing them for an incompressible liquid($\rho \approx$ Const.).

• the mass balance earns from the continuity equation:

$$\frac{\partial}{\partial t}\rho + \nabla \cdot (\rho u) = 0\,, \tag{3.1.1}$$

which in our case will be simplified to:

$$\nabla \cdot u = 0\,, \tag{3.1.2}$$

• the momentum balance deliver the Navier-Stokes equation (NSE) (Landau and Lifschitz, 1991):

$$\frac{\partial u}{\partial t} = \nu \nabla^2 u - (u \cdot \nabla) u - \frac{1}{\rho} \nabla p \cdot \tag{3.1.3}$$

The equation 3.1.2 and 3.1.3 are presenting the basic information for describing the Taylor-Couette System (TCS). As mentioned in section introduction we have assumed that in radial direction we have no-slip boundary conditions on the cylinder. Beyond of this assumption boundary condition can impose in axial direction on the system to show and describe the axial structures along of the cylinder.

$$\mathrm{u}(r1) = \begin{pmatrix} 0 \\ r_1\Omega_1 \\ 0 \end{pmatrix}, \quad \mathrm{u}(r2) = \begin{pmatrix} 0 \\ r_2\Omega_2 \\ 0 \end{pmatrix}, \quad \mathrm{u(z) = u\ (z{+}L)}\,, \quad \mathrm{p(z) = p(z{+}L)} \cdot$$

Also for implementation of equation 3.1.2 and 3.1.3 we need the following dimensionless equations in cylindrical coordinates.

• Navier-Stokes equations:

$$\begin{aligned} \frac{\partial u_r}{\partial t} &= \nabla^2 u_r - Re_i (U \cdot \nabla) u_r - \frac{u_r}{r^2} - \frac{2}{r^2}\frac{\partial u_\theta}{\partial \theta} + Re_i \frac{u_\theta^2}{r} - \frac{\partial p}{\partial r}\,, \\ \frac{\partial u_\theta}{\partial t} &= \nabla^2 u_\theta - Re_i (U \cdot \nabla) u_\theta - \frac{u_\theta}{r^2} - \frac{2}{r^2}\frac{\partial u_r}{\partial \theta} + Re_i \frac{u_r u_\theta}{r} - \frac{\partial p}{\partial \theta}\,, \\ \frac{\partial u_z}{\partial t} &= \nabla^2 u_z - Re_i (U \cdot \nabla) u_z - \frac{\partial p}{\partial z}\,. \end{aligned} \tag{3.1.4}$$

• Continuity Equation:

$$0 = \frac{1}{r}\frac{\partial}{\partial r}(r u_r) + \frac{1}{r}\frac{\partial}{\partial \theta} u_\theta + \frac{\partial}{\partial z} u_z \cdot \tag{3.1.5}$$

- Boundary Conditions (no-slip and periodicity):

$$U(r = \frac{\eta}{1-\eta}) = \begin{pmatrix} 0 \\ 1 \\ 0 \end{pmatrix}, \quad U(r = \frac{1}{1-\eta}) = \begin{pmatrix} 0 \\ 1 \\ 0 \end{pmatrix}, \tag{3.1.6}$$
$$U(z=0) = U(z=L), \quad p(z=0) = p(z=L).$$

3.2 Regimes Observed

According to the figure 1.1.3 when we increase Re_i from 0 to 500 with attention to this matter, that in our experiment Re_O is zero we can easily figure out, we face with three regimes as:

- Couette Flow,
- Taylor Vortex Flow,
- Wavy Vortex Flow.

And in this section these three regimes will be described.

3.2.1 Circular Couette Flow (CCF)

For small Reynolds numbers and without any external effect we have one purely tangential flow inside the gap between the two cylinders. In this regime and around of Cylinder axle we have profile of a laminar flow as you can see in 3.2.1. According to this matter, that the boundary conditions are symmetric, this field is rotation- and z transitionally invariant. We know this field as Circular Couette Flow (CCF), and the profile of this regime would be as follows:

$$U_{CCF} \equiv \begin{pmatrix} 0 \\ u_{\theta_{CCF}}(r) \\ 0 \end{pmatrix}, p_{CCF} \equiv p_{CCF}(r). \tag{3.2.1}$$

When we insert equation 3.2.1 in previous equation 3.1.4, then we'll get:

$$\left(\frac{1}{r}\frac{\partial}{\partial r} + \frac{\partial^2}{\partial r^2} - \frac{1}{r^2}\right) u_{\theta_{CCF}}(r) = 0 \tag{3.2.2}$$

$$Re_i \frac{u^2_{\theta_{CCF}}(r)}{r} = \frac{\partial p_{CCF}(r)}{\partial r} \tag{3.2.3}$$

With general solution:

$$u_{\theta_{CCF}}(r) = Ar + \frac{B}{r} \tag{3.2.4}$$

In previous equation A and B are integration constants, which have been drived out from equation 3.1.6, and in this case these are as follows:

$$A = -\frac{\eta^2 - \mu}{\eta(1+\eta)}, B = \frac{\eta(1-\mu)}{(1-\eta)(1-\eta^2)} \tag{3.2.5}$$

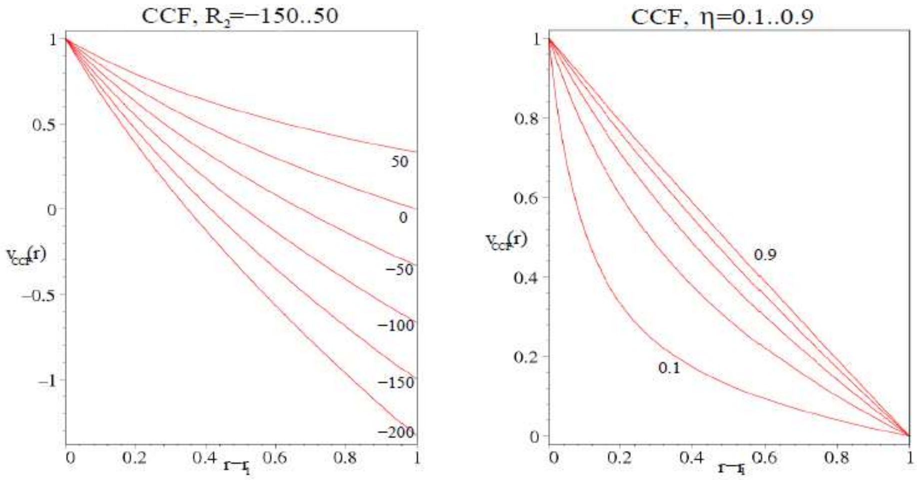

Figure 3.2.1: Influence of Re_o and η on the Velocity profile v_{CCF} of Circular Couette Flow. Control parameters: $Re_i = 150$; left: $\eta = 0{:}5$, right: $Re_o = 0$. Courtesy of Altmeyer (2011)

3.2.2 Taylor Vortex Flow

The simplest structure, which can occur over the critical area in Taylor-Couette System is the Taylor Vortex Flow (TVF). This regime is about closed toroidal vortex states, that primary is bifurcation from ground state CCF. This regime has been discoverd for the first time in year 1923 by Taylor (1923). Taylor vortexes are representing one rotational symmetric structure and also axial translation invariant structure and in this structure we'll concern about both stationary and rotational invariant solutions.

For analyzing every single structure in Taylor-Couette System all physically fields wil be shown as developed modes in azimuth (θ) and axial (z) direction as follow:

$$f(r,\theta,z;t) = \sum_{m=-\infty}^{\infty} \sum_{n=-\infty}^{\infty} f_{m,n} e^{i(m\theta+nkz)}\,, \quad f \in \Big\{u_r, u_\theta, u_z, p\Big\}. \tag{3.2.6}$$

And in this formula k is axial wave number which in our case is equal to $2\pi/L$, and also structures with azimuth wave number M contain only those modes m, which are integer multiple of M, according to the context: $m = M.n$. The velocity of this field according to the equation 3.2.6 and depending to the radial and axial coordination would be as follow:

$$f(r.\theta,z;t) = f(r;t) = \sum_{n=-\infty}^{\infty} \mid f_{0,n} \mid e^{inkz}\,, \quad f \in \Big\{u_r, u_\theta, u_z, p\Big\}. \tag{3.2.7}$$

In figure 3.2.2 (a) we can see the possible excited modes (blue square), and in this figure consequently only modes with m=0 are presented. In figure 3.2.2 (b) the spectrum of modes in one numerical calculated TVF state (Controllparameter has mentioned in figure) and specially the relative strength of exciting could be seen. The strongest and dominant mode, which is red circles and synonymous with the critical mode is arbitrarily scaled to the value of 1 here. The next higher harmonic mode is magnitude order weaker than the dominant mode. The figure 3.2.2 (c) and (d) provide information about the spatial behavior of the fields. In (C) vector plots for both fields u_r(r,z) and u_z(r,z) are in one θ=Constant plane including the false colors of azimuth vorticity ω_θ illustrated (red=Max, Blue=Min). Similarly figure (d) shows one $\theta - z$ section in the center of the gap (r=0.5) in the system and in false colors the radial field u_r is shown, which is perpendicular to the lied plane. For control parameters as used in Figure 3.2.2, the TVF structures are relatively homogeneously extended over the entire gap. However, this changes with increasing counter-rotation of the outer cylinder, which is a very general phenomenon in the Taylor-Couette system. As the counter-rotation increases, all the structures are forced ever more towards the inner cylinder.

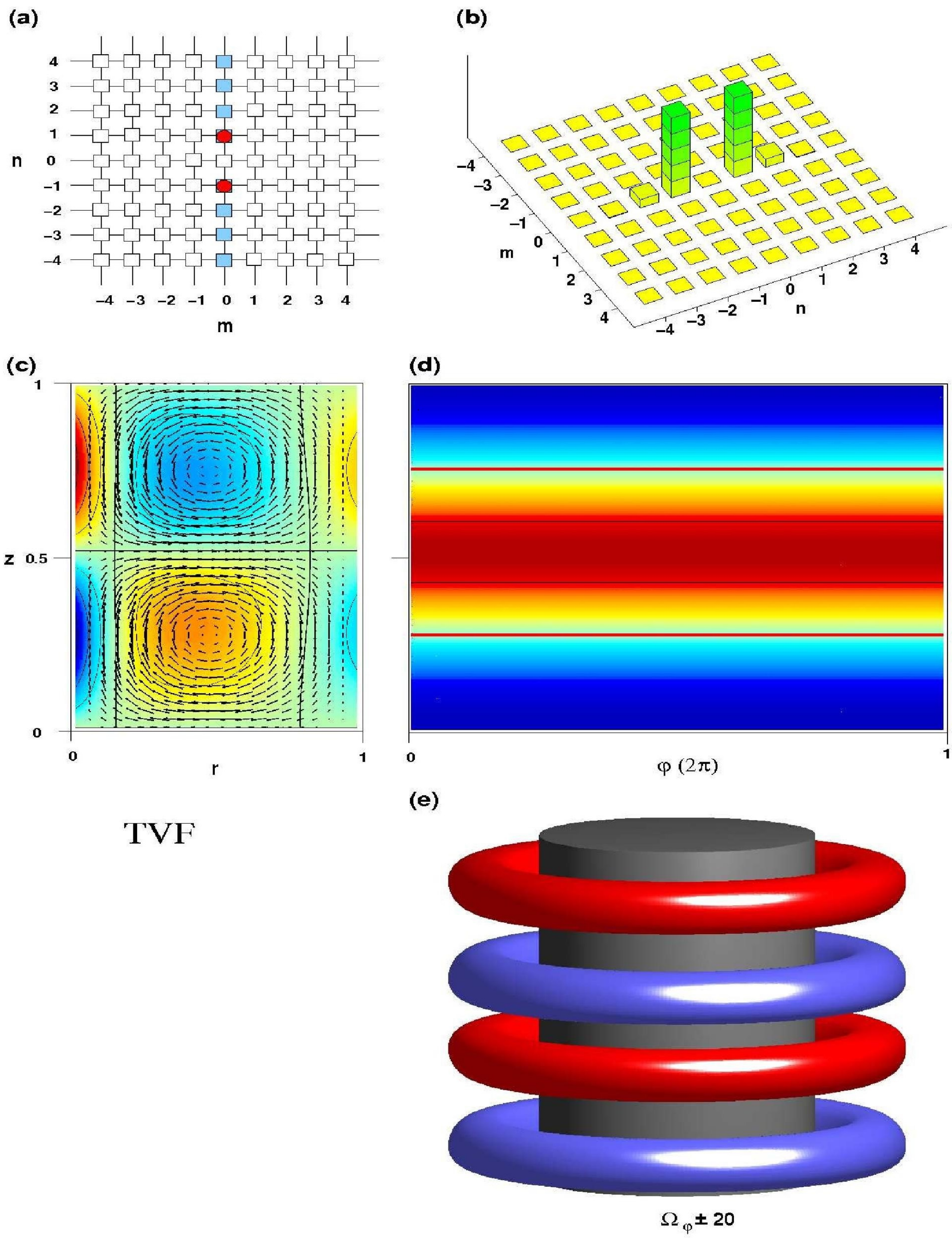

Figure 3.2.2: Characterization of a TVF state: (a) non-linear mode excitation; blue squares show the nonlinear excited modes, and the red circles the dominant modes, and respectively the modes of the linear structure. (b) u_r mode excitation.(c) vector plots of the fields u_r(r,z) and u_z(r,z) in the r-z plane (θ=const.); False colors encode the azimuthal vorticity Ω_θ (blue = max, red = min). (d) section in the $\theta - z$ plane in the middle of the gap (r = 0.5); False colors encode the radial velocity field u_r (blue = max, red = min). (e) isosurfaces of azimuthal vorticity $\Omega_\theta = \pm 20$. Control parameters: $Re_i = 80$, $Re_o = 0$, $\eta = 0.5$, $k = 3.927$.Image adopted from Altmeyer (2011)

3.2.3 Wavy Vortex Flow

Wavy Vortex Flow (WVF) structure represents one secondary bifurcating solution from the primary bifurcating TVF state. However, theoretically a primary bifurcation of this state directly out of the CCF is also conceivable, on one position of $m = 0$ and another $m \neq 0$ mode. But at least one $m \neq 0$ mode must be capable of growth, so that the structure can exist at all.

In figure 3.2.3 is one solution of 2-WVF illustrated. In (a) the involved modes are shown, while (b) shows the strength of the associated amplitudes of the field u_r. Here as the chosen example of 2-WVF state in the mode spectrum just the paired m are in fourirer space excited. It means $m = 2.n$, where the $m = 0$ are clearly the dominant modes. For completeness it should be mentioned that in the case of 1-WVF solution all m modes will be excited. The next higher excited modes ($m \neq 0$) are significantly weaker, but have an azimuthal θ and temporal t dependence in the entire structure. Basically, this is a deformed and axially distorted TVF state, similar to a wave (hence the name 'Wavy') that rotates azimuthally as a whole.

The spatiotemporal behavior of a 2-WVF state is exemplified for selected parameters in figure 3.2.3. As it can be seen in (d) and (e) the modulation of the TVF (figure3.2.2) state will be resulted to one time-dependent movement muster. This muster rotates azimuthally with a constant angular velocity in same direction like inner cylinder. For one fixed θ oscillates muster actually in axial direction, but no propagation takes place in this direction, and the oscillation in red arrows entered in (d) represent the propagation direction of the structure. For 2-WVF solution it means, that propagation doesn't move either up or down, also doesn't propagated axially, but it only rotated in the azimuthal direction.

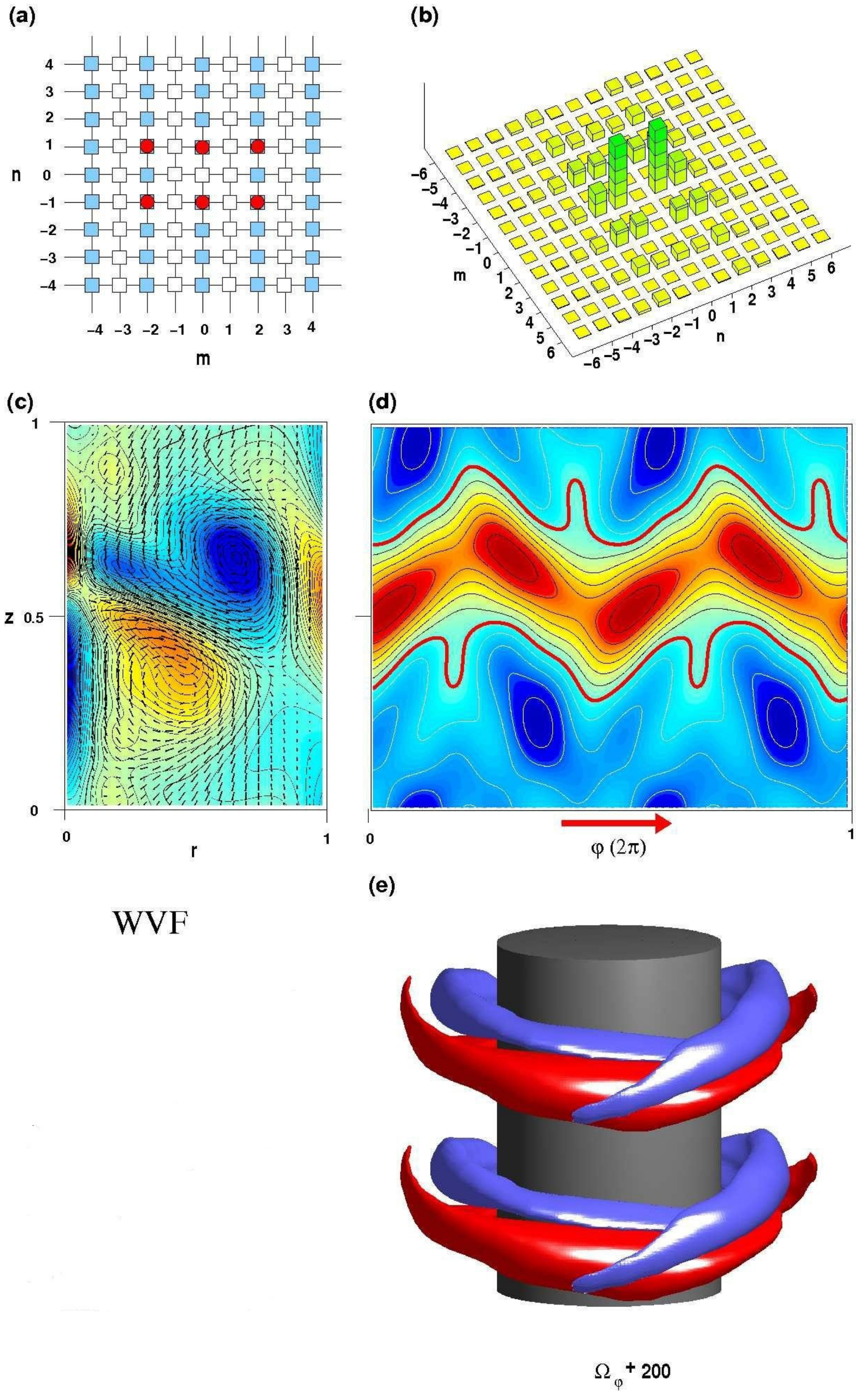

Figure 3.2.3: Characterization of the 2-WVF state: (a) non-linear mode excitation, here only m = 2n; blue squares show the nonlinear excited modes, the red circles the dominant modes, and respectively the modes of the linear structure. (b) u_r mode excitation. (c) vector plots of the fields u_r(r,z) and u_z(r,z) in the r-z plane (θ=const.); False colors encode the azimuthal vorticity Ω_θ (blue = max, red = min). (d) section in the $\theta - z$ plane in the middle of the gap (r = 0.5); False colors encode the radial velocity field u_r (blue = max, red = min). (e) isosurfaces of azimuthal vorticity $\Omega_\theta = \pm 200$. Control parameters: $Re_i = 244$, $Re_o = -150$, $\eta = 0.5$, $k = 4.2$. Image adopted from Altmeyer (2011)

3.3 Qualitative Results

As it has been mentioned in the first section of this chapter, that all the process of experiment would be described not only in a quantitative way, but also in a qualitative way. For this matter, and for proving, that all the obtained results in 16 steps of our experiment, which has been illustrated in table 2.1 could be corresponded completely to the previous investigations and mentioned literature, which has been discussed in the last section, whole process of the experiment has been recorded by one camera.

It means, that there is one captured video for every single step of the experiment, which can present properties of rotated flow (as vortex, related velocity, etc). So these videos have been imported to MATLAB first for changing to the images, then for better comparing some changes were made on them like cropping, and rotating, and finally for 6 of these steps we have made a subplot, which showed and explained us correctly changing path of the fluid in Cylinder, and also consequences of increasing the Reynolds Number.

As it has been shown below, and according to previous explanation, at the first step we have converted all 16 captured videos frame by frame to images for better observing all changes in the fluid, which rotates between cylinders in different Reynolds Numbers and also to be able to compare these images in the next steps. For this matter, all the 16 videos have been saved in 16 different folders, and with using commands num2str and strcat in one loop we defined the file names for every single videos in related folder. Then with commands VideoReader and NumberOfFrames all videos have been converted to the Frames, and finally due to the defined order in the loop all the frames have saved as a format of JPG in a specific folder.

```
fd0='C:\Users\amini\Desktop\Movies from Experiment\';
fd1 = 'Re='
fd2 = '\Video\'
fd3 = 'MVI_6800.MOV'
fd4 = 'images\IMG_';

ff  = [50,75,100,112.5,118.5,125,137.5,150,175,200,250,300,350,400,450,500];

nlist=16;                               % 16 Movies from experiment to be converted
for ilist=1:nlist
    n_string = num2str(ff(ilist));
    filename = strcat(fd1,n_string);
    disp(filename);                     % Every Reynolds number has a specific filename in the loop

    fname = strcat(fd0,filename,fd2,fd3); % Selecting the videos in the folders

    v = VideoReader(fname);
    numFrames = v.NumberOfFrames;       % Using commands VideoReader & NumberOfFrames to read & convert the videos to frames
    n=numFrames;
    for i = 1:1:n                       % change intermediate value to chnage the sampling frequency
        J = read(v,i);
        imshow(J)
        fname=strcat(fd0,filename,fd2,fd4,num2str(i),'.JPG');
        imwrite(J,fname);               % save without frame
    end

    disp('Preliminary data to be included in my_database:\n')
    disp(strcat('init=',num2str(1)))
    disp(strcat('end=',num2str(n)))
    load(fname)

end
```

In next Step some extra editions have been done on the all captured images, and after observing all the images it has been decided, that for 6 Reynolds Number, which are Re = 75, 125, 150, 175, 300 and 500, one Subplot should be issued, that clearly illustrates fluid changes within the cylinder in different phases. In follow the related command has been shown.

```
f0 = 'C:\Users\amini\Desktop\Movies from Experiment';
f1 = '\Re=';
f2 = '\Video\images\';
f3 = 'IMG_';
f4 = 'Crop\Crop_';
ff = [50,75,100,112.5,118.5,125,137.5,150,175,200,250,300,350,400,450,500];

for i = 16:-1:1
    n_string = num2str(ff(i));
    filename = strcat(f1,n_string);
    disp(filename);                     % Every Reynolds number has a specific
                                          filename in the loop
    n=1514;                             % Number of images in every folder

    aa = strcat(f3,num2str(1));
    A = strcat(f0,filename,f2,aa,'.jpg');
    J=imread(A);                        % Commad for reading all the images

    imshow(J);
    [x, rect] = imcrop(J);              % Croping images and saving the coordination
    load('cordinate.mat')
for b=1:1:n
    cc = strcat(f3,num2str(b));
    A = strcat(f0,filename,f2,cc,'.jpg');
    J=imread(A);
    I = imcrop(J,rect);
    S = imrotate(I,-90);                % Rotating the images counterclockwise

    B = strcat(f0,filename,f2,f4,num2str(b),'.jpg');
    imshow(S);
    imwrite(S,B)
end
    save cordinate.mat rect
end

f5 = '\Subplot\Subplot_';
ff = [75,125,150,175,300,500];         % Choosing 6 selected Reynolds number

i = 1:1:6;

for j = 726:1:825                       % 200 Images between 726 and 825 has been
                                          selected for the purpose of creating the
                                          movie
    figure(j);

for i=1:1:6

    h = subplot(2,3,i);                 % Creating Subplot with 2 rows & 3 columns

    n_string = num2str(ff(i));
    filename = strcat(f1,n_string);
    disp(filename);

    A = strcat(f0,filename,f2,f4,num2str(j),'.jpg');
    B = imread(A);
    imshow(B)

    title ('filename')
    xlabel('120 [mm]')
    ylabel('72 [mm]')
    set(h, 'Position', [.05 .55 .25 .3]); % Setting a specific position for every
                                            plot
    set(gca, 'LineWidth',1,'TickLength' ,[0 0]) % Setting Linewidth & TickLength
                                                  for every plot
    set(gca, 'Layer', 'top')
    axis on
    xticklabels({})
    yticklabels({})
end
    C = strcat(f0,f5,num2str(j),'.png');
    print('-dpng',C,'-r1200')            % Printing the Subplot as a format of .png
end
```

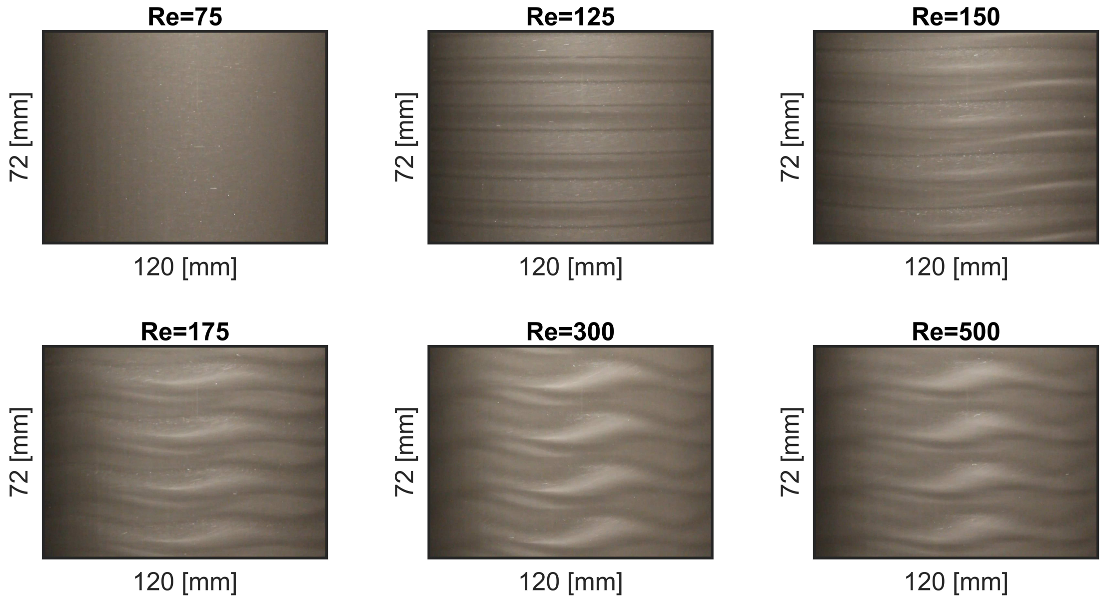

Figure 3.3.1: A figure for a fluid within Taylor Couette Cylinder corresponding to 6 different values of the Reynolds Numbers, indicated on top of each panel.

As it shown in figure 3.3.1, there is a figure with 6 images, which presents the flow in 6 different circumstances. First image from top left is about a flow in $Re = 75$. Clearly it can be said, that in this phase, there are no vortices or cell in entire of the cylinder, and according to the figure 1.1.3 it could be said, that flow structure in this phase is related to circular couette flow (CCF), which has been discussed in subsection 3.2.1. With increasing the rotation velocity of inner cylinder, while our Taylor Number crosses from critical Taylor Number (T_C), which has been defined in formula 2.1.3 with a value equal to 1837.925 in our case, it could be estimated, that the flow would be changed to a system with a regular vortices. With Attention to the image at top middle, this estimation has been completely proved, because in this step ($Re = 125$) Taylor Number is equal to 2063.679, which is beyond the mentioned critical Taylor Number, and it's obviously clear to expect this type of flow structure.

Increasing further the rotation rate of inner cylinder around the $Re = 150$, as it illustrated in the image at the top right, and with attention to the diagram phase, it could be figured out, that the flow is now in phase of Taylor Vortex Flow (TVF), as it has reported in subsection 3.2.2. In this phase it could be concluded, that there are some nonlinear modes or vortex in the flow, but somehow the dominant modes are still the linear modes, and we have still one linear structure, something that could be seen also in the related image.

When Reynolds Number increases further, and crosses beyond of that, the new phase of flow will be arisen. This phase, as it was discussed in subsection 3.2.3 is Wavy Vortex Flow. As it could be watched, the three images in the below row with Reynold Number $Re = 175$, 300 and 500, respectively, are in phase of Wavy Vortex Flow. It's quite clear, that in these Reynolds Numbers there is no sign of linear modes, but just non linear modes, making the non linear structures for the flow. Of course with attention to the images this claim can be acknowledged.

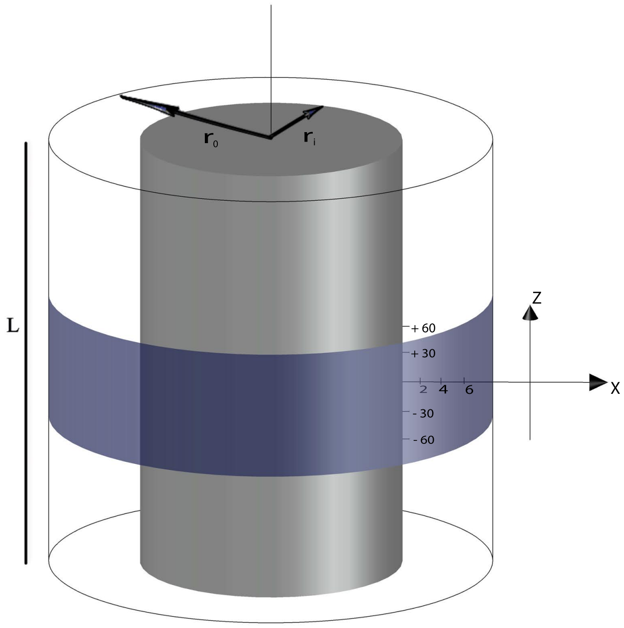

Figure 3.3.2: Schematic sketch of Taylor-Couette Cylinder with describing the configuration and measurement points, with indication of the area considered.

3.3.1 Steady State Results

In this section the time-averaged results from experiment are going to be considered and analyzed. It means all the obtained results, which are the time depended, for ten different Reynolds number (100,112.5,125,137.5,150,175,200,300,400, and 500) are imported to the program MATLAB, and the output is going to be sorted and plotted in two radial velocity and Tangential velocity category.

For this matter, it should be referenced to the first type of results, which has been illustrated in figure 2.3.1 (a). In the first observing, it should be came up, that this type of results have 15 columns and 183 rows. First what should be considered, is the first three columns, that are presenting the coordinates points of measurement, and it could be seen, along the direction of cylinder radius (X direction), three points has been defined as: 2, 4, and 6mm, also 31 points along the cylinder axis (Z direction) from -60 to 60 ($-60 : 2 : 60$)mm as it has been drawn in figure 3.3.2. Then mean velocities have been measured in these points. So these captured velocities have been analyzed, and results are shown in the plots, as shown in following.

So in the first figure 3.3.3 as it shows, the one mean value for the columns 8th, 10th, 12th, and 14th, which presenting the radial mean velocity in point 2, have been chosen, and they are compared to the mean value from the columns 9th, 11th, 13th, 15th, which are related to tangential velocities in the same point. For sure and as it is expected, all mean velocity in Tangential direction are greater than the mean velocity in radial direction. Also for the radial and tangential velocity in the desired columns two figures over the three different values of X are shown, which all the mean velocity in desired columns were drawn, and comparing to each other, as it shown in figure 3.3.4, and 3.3.5.

With the first attention it could be recognized, that in all the issued figures there are traces of the flow transition at the related Reynolds numbers. For example in figure 3.3.5 at the $X = 4$ and before the $Re = 150$ we can see the points, which have been shown in figure are out of the trend. Reason for this phenomenon is for the transition of the flow regime form CCF to the TVF, also around the $Re = 300$ we can see this difference, which is also about the flow transition from TVF to the WVF, and it shows, that our analyses on the obtained results are fully corresponded to the qualitative results in last section.

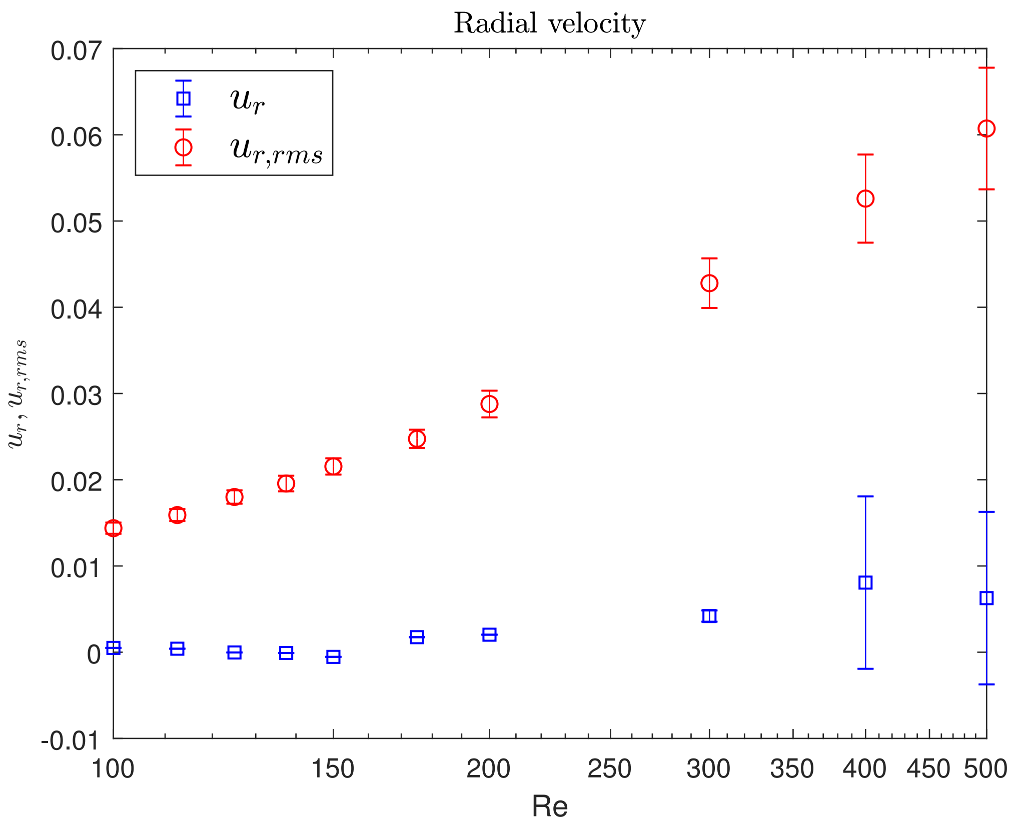

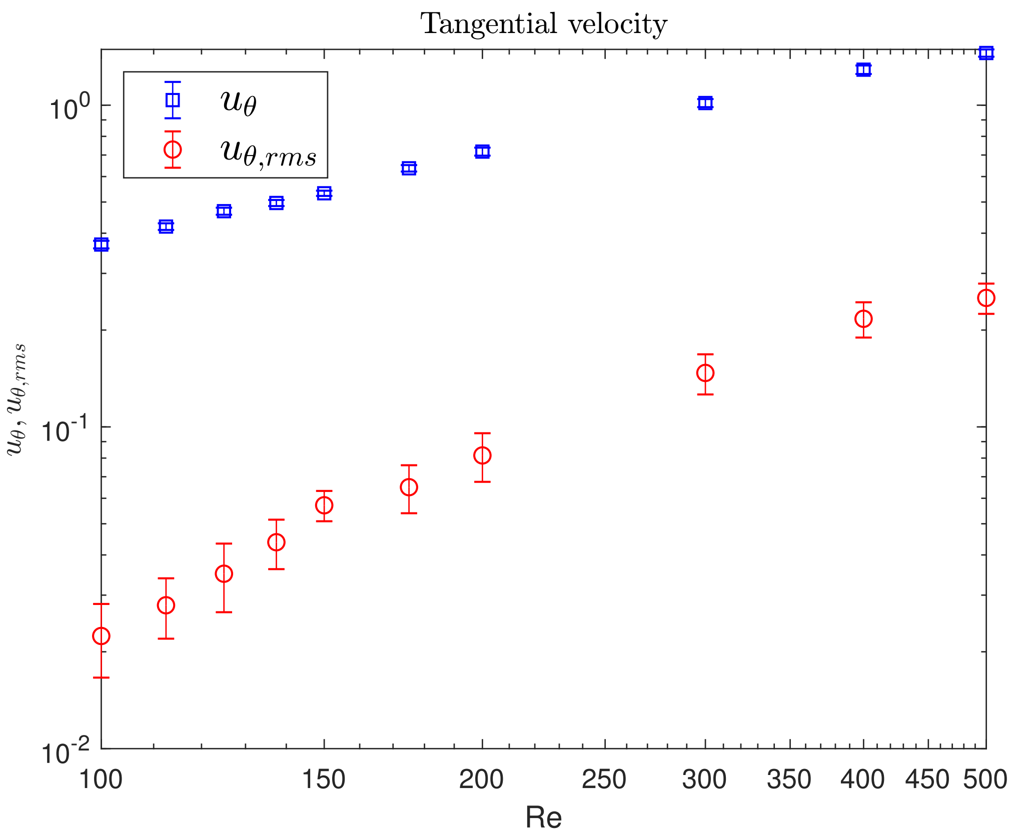

Figure 3.3.3: Comparison of the mean velocity and root mean square velocity for Radial and tangential direction over the Reynolds numbers at the position X = 2.

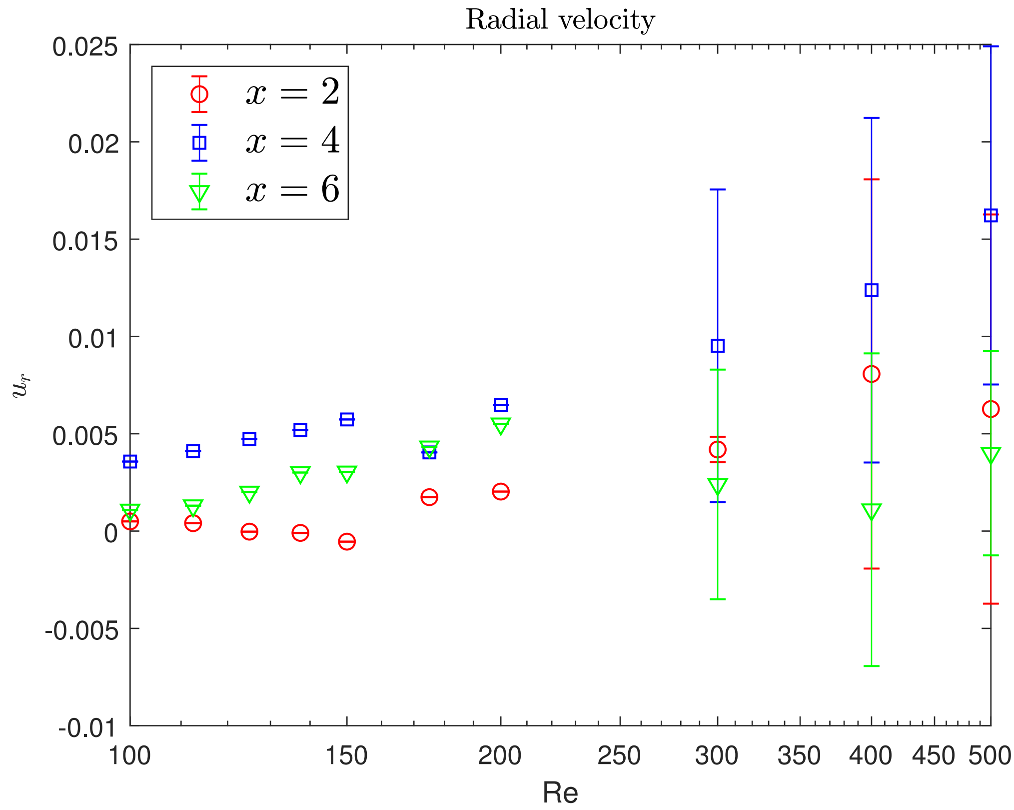

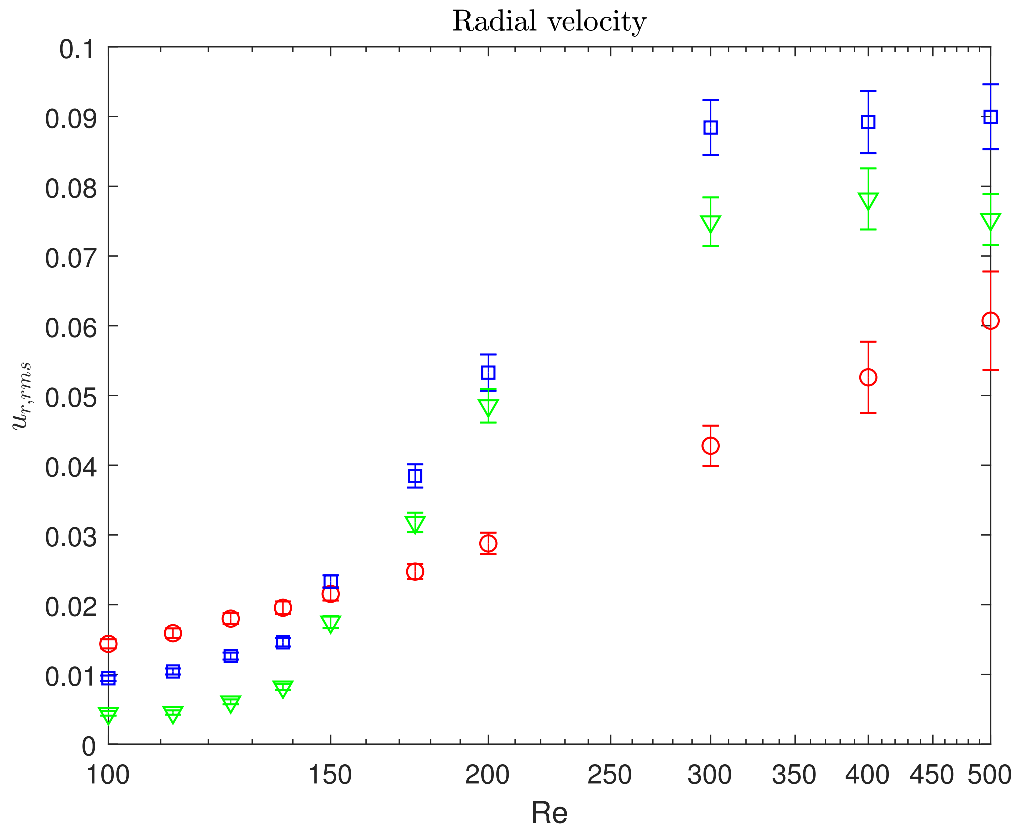

Figure 3.3.4: Comparison of the Radial mean velocity and Radial root mean square velocity over the Reynolds Numbers according to the values in three position of X (X =2, 4 and 6).

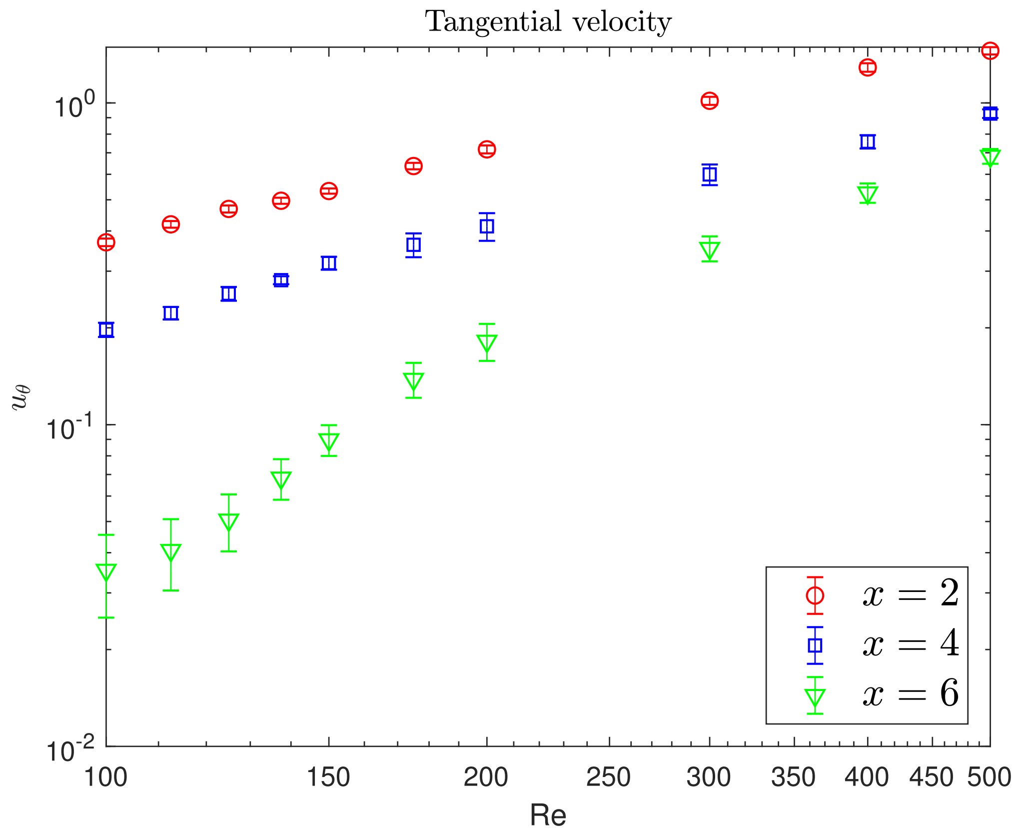

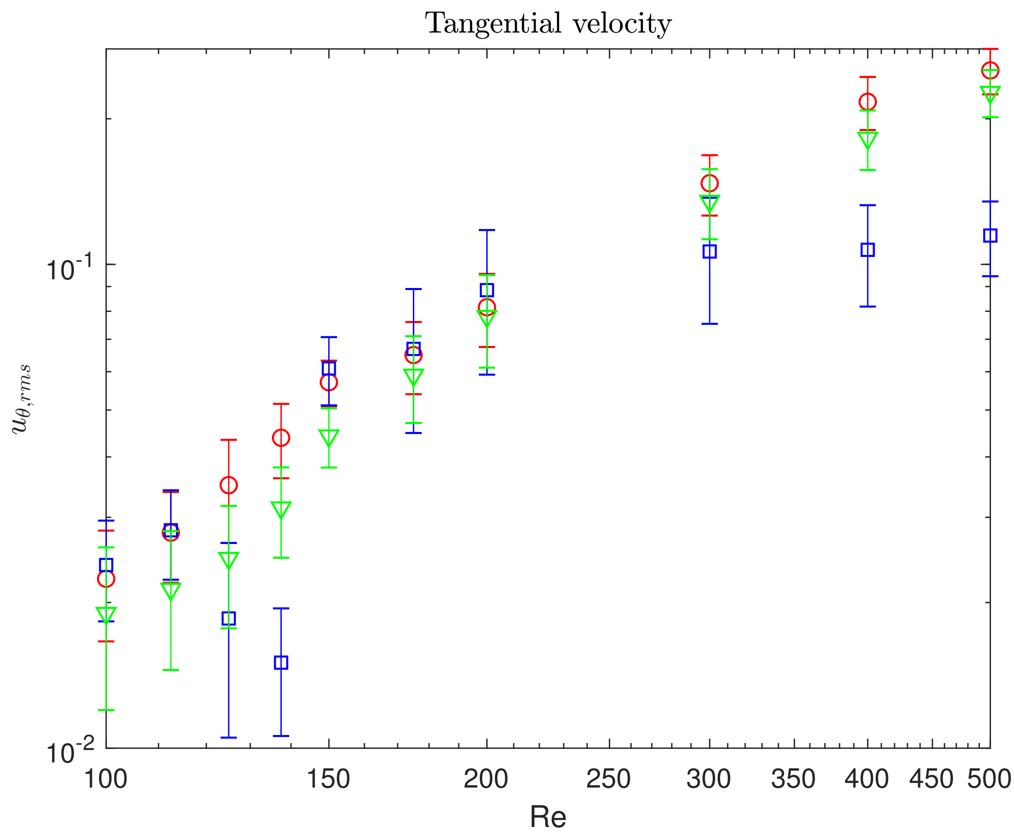

Figure 3.3.5: Comparison of the Tangential mean velocity and Tangential root mean square velocity over the Reynolds Numbers according to the values in three position of X (X =2, 4 and 6).

3.3.2 Time-Dependent Analysis

In this subsection the obtained results from the experiment, which is related to the Reynolds numbers 75, 125 and 300, will be discussed. As it reported in last section two types of results have been derived out regarding to the measurement of mean velocity and instantaneous velocity within Taylor-Couette Cylinder. In section 2.3.2 it has been described, how the captured data from experiment have been converted from time domain signal to the frequency domain signal, and then how with attention to data for the second type of text file, which is relevant to the measurement of instantaneous velocity in the cylinder, some diagrams like the figure 2.3.3 for every Reynolds number could be figured out.

So three Reynolds number (75, 125 and 300) have been chosen, due to their different structure, and at the first step the three most dominant frequencies from the mentioned Reynolds number were selected for comparing to each other. For this matter first value Z was defined as bellow:

$$Z = N_z * \frac{h}{60}, [m] \tag{3.3.1}$$

which h = 0.120 (m) is the height of cylinder, N_z is number of selected points from $-30 : 2 : 30$, which is 31 and digit 60 is distance between the points at the top and bottom of the cross section.

Therefore in the first issued diagram the first three dominant amplitude were compared to each other with respect to the defined value Z, as it shown in figure 3.3.6. But it should be explained, that from the corresponding text file as it shown in the part b of figure 2.3.1 the values in the first column, which presenting radial velocity are calculated at the first time, then at the second time the values in the fourth column, which presenting the tangential velocity are calculated, and finally the plots have been issued in logarithmic scale.

According to what can be seen in figure 3.3.6, it's completely obvious that as long as Reynolds number increases for tangential velocity and also radial velocity the most dominant amplitude also increases, but with attention to Reynolds number 300, it can be also figured out, that the second and third dominant frequencies have an amount more than the same in Reynolds number 75 and 125, and for sure the reason is about the structure of the flow in this phase.

In figure 3.3.7 three first dominant frequency and also amplitude were compared with each other. What clearly could be received in the first look in radial velocity, is that, the most dominant mode has been increased as long as the Reynolds number increases. Also at Re=125 for the second dominant mode in radial velocity, it could be concluded, that it has more value in compare to the third mode, however this difference is not too large, but it can be seen in figure. But this order can not be seen in Re=75, and the second and third modes have almost the same value in amplitude, but with different frequency.

In tangential velocity figure it shown, that the dominant modes, which are related Re=300 have almost same frequency, but they are much more from the same in Re=75,125. Also it shows obviously, that in Re=75,125 we have almost same amplitude for the modes, but in a Wider range of frequency.

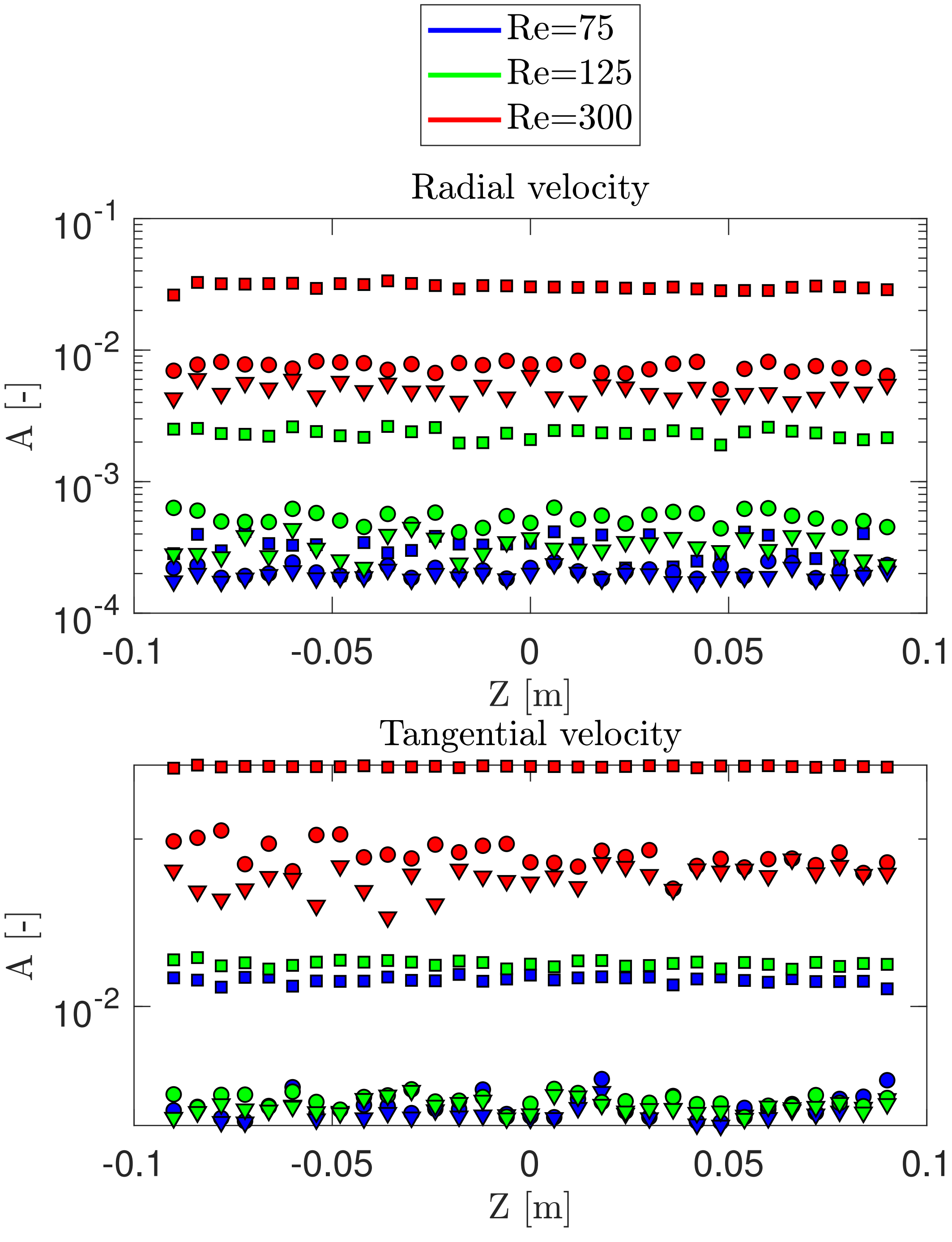

Figure 3.3.6: Comparison of the Tangential velocity and Radial velocity for Reynolds number 75, 125 and 300 according to the first three dominant amplitude. Symbol square (□) shows the first dominant mode, circle (○) second dominant mode and Symbol triangle down (▽) third dominant mode.

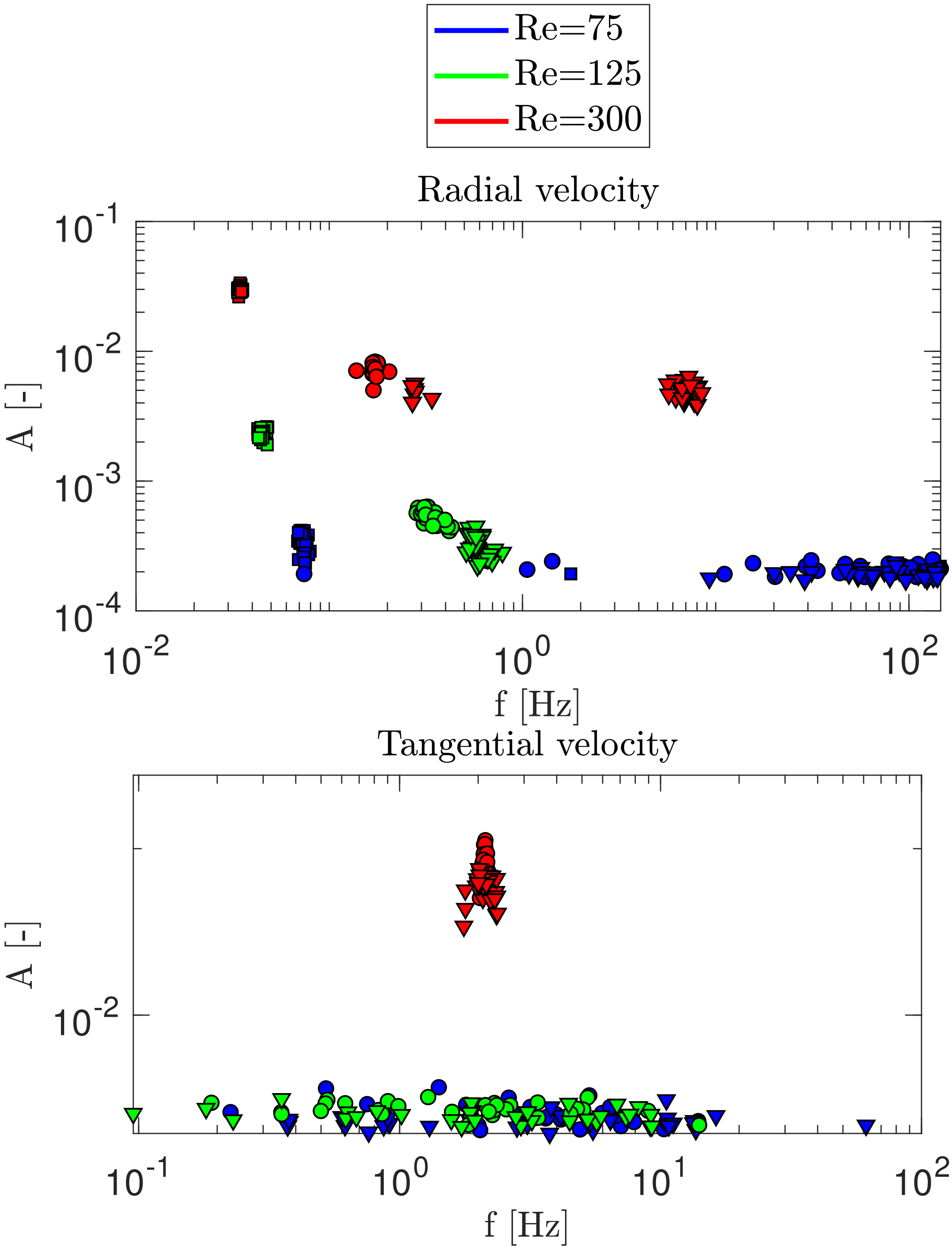

Figure 3.3.7: Comparing the Tangential velocity and Radial velocity for Reynolds number 75, 125 and 300 according to the first three dominant amplitude. Symbol square (□) shows the first dominant mode, circle (○) second dominant mode and Symbol triangle down (▽) third dominant mode.

As it shown in figures 3.3.8, the radial- and tangential velocity at the all measurement points in 3 different Reynolds number has been drawed. For plotting this figure, first in the related command in MATLAB one matrix has been defined related to every figure, then all the values from desired section were gathered in this matrix,which for the tangential velocity the values has been collected from the first column of resulting text file and for the radial velocity from the fourth column of resulting text file. Then the capturing matrix, that is fp2 and fp2-1 was divided to number of points,which gives the color charts and finally order to plot it in logarithms scale, as it described below.

```
    fp2=zeros(1,1800);          % Defining one Matrix with one row & 1800 columns
    fp2_1=zeros(1,1800);

for i=1:31                      % set a loop for 31 Points of measuring
    fp2=fp2+s(j).fp(2,1:1800); % Adding the desired values from the captured structure to defined Matrix
    fp2_1=fp2_1+s(j).fp_1(2,1:1800);

end
    fp2=fp2/31;                 % dividing the added values to the number of points
    fp2_1=fp2_1/31;


    plot(s(1).fp(1,1:1800),s(1).fp(2,1:1800),'-k')     % Plot Matrix fp & fp2
    plot(s(1).fp(1,1:1800),fp2,strcat('-',col(i)))

    hold all
    plot(s(1).fp_1(1,1:1800),s(1).fp_1(2,1:1800),'-k') % Plot Matrix fp_1 & fp2_1
    plot(s(1).fp_1(1,1:1800),fp2_1,strcat('-',col(i)))

    box on
    set(gca,'Xscale','log','Yscale','log') % set the figure in logarithms scale
    xlabel('f [Hz]')
    ylabel('A [-]')
    hl=legend(strcat('Re=',num2str(ff(1))),... % set a legend for three Reynolds number
        strcat('Re=',num2str(ff(2))),...
        strcat('Re=',num2str(ff(3))));
    set(hl,'location','northwest','interpreter','latex','fontsize',fs)
```

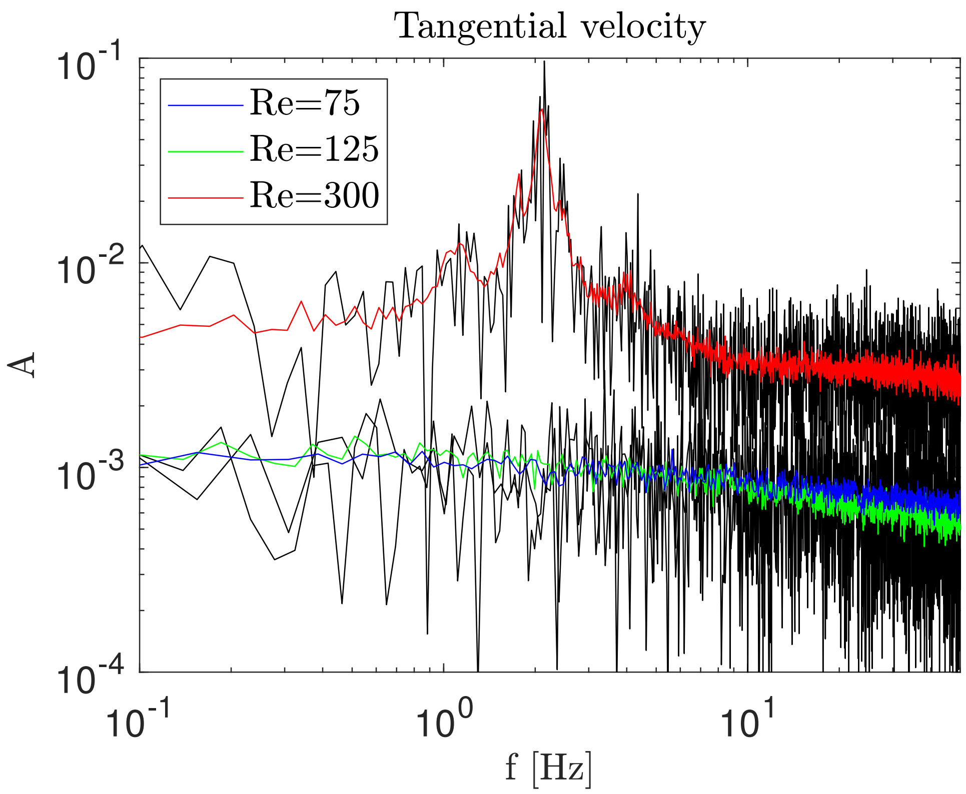

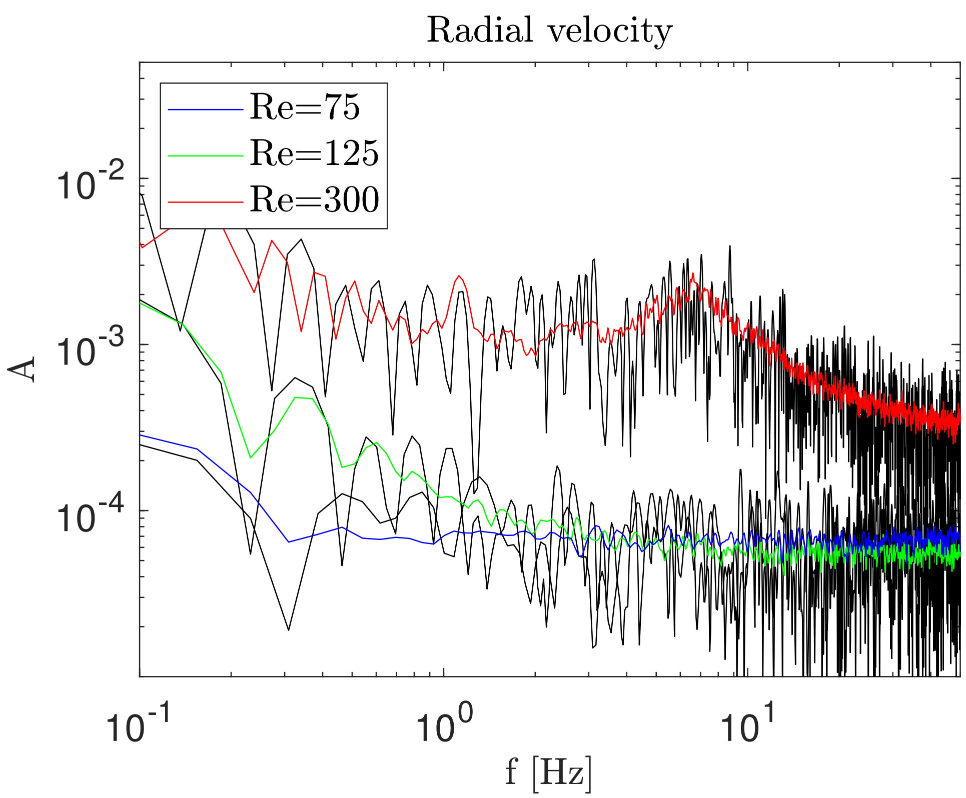

Figure 3.3.8: Figures related to Radial and Tangential velocity for Re = 75, 125 and 300. Black lines show the instantaneous velocity at the every measurement point in Z direction. Colored lines are average of instantaneous velocity over Z axis.

4. Conclusion

Behaviour of flow transition is a complex phenomenon. In order to investigate their motion and dynamics and obtained related information, an experimental design with a flow is considered. In this work, we analyzed experimentally the Taylor-Couette flow, i.e. the flow observed between two concentric and rotating cylinders. This experimental setup represents one of the archetypal problems for the study of turbulent flows with and without heat exchange, and it is a good candidate for the investigation of the ultimate regime of turbulent convection.

We performed experiments at 16 different values of Reynolds number (i.e. 16 different values of Taylor number) with the facility available at the Institute of Fluid Mechanics and Heat Transfer. We used the facility in the configuration in which only the inner cylinder rotates, whereas the outer cylinder is kept fixed. Within the range of parameters explored, we observed three different regimes. The flow behaviour in these regimes has been analyzed both qualitatively and quantitatively, via particles visualisation techniques and velocity statistics respectively.

The main object of this work consists of the development of a set of MatLab-based numerical tools for the processing, analysis and visualisation of the flow velocities. The tools developed allow the analysis of the data obtained from Laser Doppler Anemometry (LDA) measurements. In particular, two different set of analysis are now possible: steady-state and time-dependent analyses. The former allows a characterisation of the mean properties of the flow, with precise information about local mean properties (mean velocities and rms'). The latter, more reach of information, is used to identify the dominant flow structures by mean of the Fast Fourier Transform (FFT). In particular, the tools developed here can handle and produce velocity statistics of measurements preformed in correspondence of different radial and axial positions.

In this work, only few of the possible Taylor-Couette flow regimes have been explore. As a further development of the present study, we plan to investigate more in detail the regimes already observed and to extend this analysis. In particular, we plan:

- To increase the Reynolds and Taylor numbers by increasing the angular velocity applied to the cylinders
- To investigate the configuration in which both cylinders are both in co- and counter-rotating.

A. Baysilone Fluid M20

Baysilone Fluid M20 is a fluid with a low-viscosity and due to it's special properties (high and low-temperature stability, a low pour point, minimum effect of temperature and pressure on viscosity, low vapour pressure, favourable dielectric characteristics little influenced by temperature and frequency, high interfacial tension to water and organic polymers, high surface activity, high compressibility, chemical and physiological inertness), it could be appropriate for heat transfer media, hydraulic fluids, liquid dielectrics, water repellents, polishes, mould release agents, lubricants, antifoams, damping fluids, auxiliaries for the manufacture of cosmetics and pharmaceuticals(Bayer, 2015).

A.1 Technical Data

Chemical properties of Baysilone Fluid M20 is a linear Polydimethylsiloxanes (PDMS), see figure A.1.1 .By adjusting -Si-O- chain lengths, the functionality of the side groups and the crosslinking between molecular chains, silicones can be synthesized into an almost infinite variety of materials.However, the linear and cyclic oligomers obtained by hydrolysis of the dimethyldichlorosilane have too short a chain for most applications. They need to be condensed (linears) or polymerised (cyclics) to give macromolecules of sufficient length Silicones-Europe (2015). Polydimethylsiloxanes is the basic and most commonly available silicone. It has a properties like not scarcely be affected by pressure like the other mineral oils, act as Newtonian fluids at viscosities below 0.001 $m^2.s^{-1}$ up to a shear rate of over 5.10^3 s^{-1}, low setting points and vapour pressures, high flash points, practically unlimited stability at temperatures of up to 150°C as you can see in technical Data table of A.1. Thermal conductivity of Baysilone Fluids M is not affected by temperature. Even the level of viscosity has only a slight effect. Thus, although the coefficient of thermal conductivity λ increases somewhat from the low to the medium-viscosity oils, it undergoes no further change when the high-viscosity grades are reached. Gases have a relatively high solubility in Baysilone Fluids M, and this is scarcely affected by temperature. The differences in solubility between the individual Baysilone Fluids M are also relatively small(Bayer, 2015).

Climatic changes have no influence on the properties of Baysilone Fluids M. When properly stored, they are stable for many years; they neither precipitate any solids, even after long periods of time, nor undergo any changes in colour or acid value. As a result of their extremely low vapour pressure, their low pour point and their absolute inertness to packaging materials, there are no special requirements with regard to storage vessels and conditions. As with any other oily fluid, contact with water generally results in emulsion turbidity(Bayer, 2015).

Specifically about the application of Silicon Oil M20 briefly we can mention that, SilOil M20.195/235.20 can be used in the range from -20 °C to +195 °C (for open systems) and to +235 °C in connection with externally sealed systems (for Unistat). It should be borne in mind that, at high temperatures, SilOil M20.195/235.20 can likewise be chemically altered by oxidising media, such as air, or substances with a catalytic effect, such as acids, lyes and various metal compounds. An increase in viscosity, and possibly even gelling of the fluid owing to crosslinking reactions, must be expected in the presence of oxidising agents, while contact with products having a catalytic effect usually induces a process of depolymerisation, resulting in a drop in viscosity (Huber, 2011).

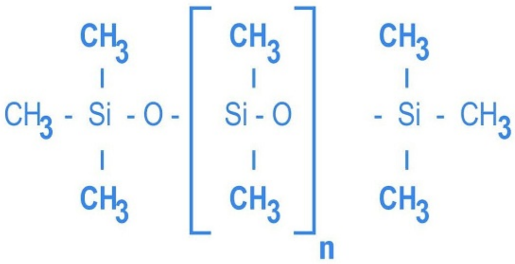

Figure A.1.1: Chemical Composition of PDMS. Courtesy of Silicones-Europe (2015)

Chemical Name:	polydimethyl siloxane
Appearance:	Clear, colourless Liquid
Vapor Pressure between 25°C and 175°C:	$\approx 10^{-5}$ and 10^{-4} mbar
Water Content:	$\approx$ 50 ppm
Refractive index at 25°C:	1,401
Setting Point (DIN 51597):	$\approx$ -70°C
Flash Point (DIN 51376:	$\approx$+240°C
Burning Point (DIN 51376):	$\approx$+290°C
Ignition Temperature (DIN 51794):	>+400°C
Mean cubic expansion coefficient in Range 25°C to 175°C:	99 and 111.10^{-5}/K

Table A.1: Technical Data sheet for Bayer Silicones Baysilone Fluids. Courtesy of Bayer (2015)

B. Aluminium Flakes Particles

As it known Aluminum in general has a low density and ability to resist against corrosion through the phenomenon of passivation. Aluminium and its alloys are vital to the aerospace industry and important in transportation and building industries, such as building facades and window frames. The oxides and sulfates are the most useful compounds of aluminum. But the particle, that has been used in our experiment was Aluminium fine powder with stabilization about 2% fat.

Formula of the substance is Al(Hill) and has a molar mass 26.98 g/mol. This product is chemically stable under standard ambient conditions (room temperature). This substance has most relevant uses for development and research and chemical production. This substance is a flammable solid and in contact with water releases flammable gases according to category 1 (H228) and category 2 (H261), respectively. So it should be keep away from heat, sparks, open flames and hot surfaces, and should be stored not in a moisture conditions, but in a closed and dry container (Merck-Group, 2018). In table B.1 information on basic physical and chemical properties has been listed.

Chemical Name:	Aluminium fine powder, stabilized about 2% fat
Appearance:	odourless, metallic powder
Melting Point:	660°C
Boiling Point:	2.467°C at 1.013 hPa
Density:	2.70 g/cm3 at 20 °C
Water Solubility:	at 20°C(reaction)
Ignition Temperature:	>+400°C

Table B.1: Technical Data sheet for Aluminium fine powder. Courtesy of Merck-Group (2018)

Bibliography

Altmeyer, S. (2011). Untersuchung von komplexen wirbelströmungen mit newtonschem fluid und ferrofluiden im taylor-couette system. *Dissertation an der Universität des Saarlandes*.

Andereck, C. D., Liu, S., and Swinney, H. L. (1986). Flow regimes in a circular couette system with independently rotating cylinders. *Journal of Fluid Mechanics*, 164:155–183.

B. Eckhardt, S. G. and Lohse, D. (2007). Torque scaling in turbulent taylor-couette flow between independently rotating cylinders. *Journal of Fluid Mechanics*, 581:221–250.

Bayer, A. (2015). *Bayer silicones Baysilone fluids M*. Edition: 7.96.

Chandrasekhar, S. (1981). *Hydrodynamic and Hydromagnetic Stability*. Dover Publication , INC New York.

Dantec-Dynamics (2000). *Particle Image Velocimetry (PIV)*. `https://www.dantecdynamics.com/particle-image-velocimetry/` [Accessed: 29.01.2019].

Edwards, W. S. (1990). Linear spirals in the finite couette-taylor problem. In *Instability and Transition*, pages 408–425. Springer.

Edwards, W. S. (1991). New stability analyses for the couette-taylor problem. *The University of Texas at Austin*.

Engine-Research-Center (2015). *Laser Doppler Velocimentry*. `https://www.erc.wisc.edu/ldv.php/` [Accessed: 30.01.2018].

Grossmann, S. and Lohse, D. (2000). Scaling in thermal convection: a unifying view. *J. Fluid Mech.*, 407:27–56.

Grossmann, S., Lohse, D., and Sun, C. (2016). High–reynolds number taylor-couette turbulence. *Annual review of fluid mechanics*, 48:53–80.

Huber, P. (2011). Technical datasheet siloil m20.195/235.20. *Peter Huber Kältemaschinenbau GmbH*, 1.

Landau, L. and Lifschitz, E. (1991). Hydrodynamik., akademie verlag.

Lathrop, D. P., F. J. and Swinney, H. S. a. (1992a). Turbulent flow between concentric rotating cylinders at large reynolds number. *Physical Review Letters*, 68(10):1515–1518.

Lathrop, D. P., F. J. and Swinney, H. S. b. (1992b). Transition to shear-driven turbulence in couette-taylor flow. *Physical Review Letters*, 46(10):6390–6405.

Lewis, G. S. and Swinney, H. L. (1999). Velocity structure functions, scaling, and transitions in high-reynolds-number couette-taylor flow. *Phys. Rev. E*, 59(5):5457–5467.

Lohse, D. and Xia, K.-Q. (2010). Small-scale properties of turbulent rayleigh-benard convection. *Journal of Fluid Mechanics*, 42:335–364.

Merbold, S., Brauckmann, H., and Egbers, C. (2013). Torque measurements and numerical determination in differentially rotating wide gap taylor-couette flow. *Physical Review E*, 87(2):023014.

Merck-Group (2018). *Aluminium fine powder*. Version 7.11.

Paoletti, M. and Lathrop, D. (2011). Angular momentum transport in turbulent flow between independently rotating cylinders. *Physical review letters*, 106(2):024501.

Pfister, G., S. H. C. K. A. and Mullin, T. (1988). Bifurcation phenomena in taylor-couette flow in very short annulus. *J. Fluid Mech.*, 191:1–18.

Siemens (2019). Product lifecycle management software inc, *Time-to-frequency.* https://community.plm.automation.siemens.com/t5/Testing-Knowledge-Base/Digital-Signal-Processing-Sampling-Rates-Bandwidth-Spectral/ta-p/402991?lightbox-message-images-402991=44367i96607A3217393B29/ [Accessed: 05.02.2019].

Silicones-Europe (2015). *Silicone Oil M20.* https://www.silicones.eu/science-research/chemistry/polydimethylsiloxanes-pdms/ [Accessed: 03.02.2019].

Stefani, F., Gundrum, T., Gerbeth, G., Rüdiger, G., Schultz, M., Szklarski, J., and Hollerbach, R. (2006). Experimental evidence for magnetorotational instability in a taylor-couette flow under the influence of a helical magnetic field. *Physical review letters*, 97(18):184502.

Taylor, G. I. (1923). Viii. stability of a viscous liquid contained between two rotating cylinders. *Philosophical Transactions of the Royal Society of London. Series A, Containing Papers of a Mathematical or Physical Character*, 223(605-615):289–343.

Tokgoz, S., Elsinga, G. E., Delfos, R., and Westerweel, J. (2012). Spatial resolution and dissipation rate estimation in taylor–couette flow for tomographic piv. *Experiments in fluids*, 53(3):561–583.

Van Gils, D. P., Bruggert, G.-W., Lathrop, D. P., Sun, C., and Lohse, D. (2011). The twente turbulent taylor–couette (t3c) facility: strongly turbulent (multiphase) flow between two independently rotating cylinders. *Review of scientific instruments*, 82(2):025105.

Van Gils, D. P., Huisman, S. G., Grossmann, S., Sun, C., and Lohse, D. (2012). Optimal taylor–couette turbulence. *Journal of fluid mechanics*, 706:118–149.